Conserved heterodimeric GTPase Rbg1/Tma46 promotes efficient translation in eukaryotic cells

Fuxing Zeng [1, 2], Xin Li [2], Melissa Pires-Alves [1], Xin Chen [3], Christopher W. Hawk [1] and Hong Jin [1,3,4*]

*Corresponding author

Addresses:

1. Department of Biochemistry, University of Illinois at Urbana-Champaign, 600 S. Mathews Avenue, Urbana, IL 61801

2. Department of Biology, School of Life Science, Southern University of Science and Technology, No. 1088 Xueyuan Blvd, Shenzhen, P.R. China 518055

3. Center for Biophysics and Quantitative Biology, University of Illinois at Urbana-Champaign, 600 S. Mathews Avenue, Urbana, IL 61801

4. Carl R. Woese Institute for Genomic Biology, 1206 West Gregory Drive, University of Illinois at Urbana-Champaign, 600 S. Mathews Avenue, Urbana, IL 61801

Phone: (217)244-9493

Fax: (217)244-5858

Email: hjin@illinois.edu

ABSTRACT

Conserved developmentally-regulated GTP-binding (Drg) proteins and their binding partner Dfrp proteins are known to be important for embryonic development, cellular growth control, differentiation and proliferation. Here, we report that the yeast Drg1/Dfrp1 ortholog, Rbg1/Tma46, facilitates translational initiation, elongation and termination via suppressing prolonged ribosome pausing. Consistent with the genome-wide observations, Rbg1 reverses the growth defect resulting from translation stalling and stabilizes mRNAs against no-go decay. Furthermore, we provide a cryoEM structure of the 80S ribosome bound with Rbg1/Tma46 that reveals the molecular interactions responsible for Rbg1/Tma46 function. The Rbg1 subunit binds to the GTPase association center of the ribosome and the A-tRNA, and the N-terminal zinc finger domain of Tma46 subunit binds to the 40S, establishing an interaction critical for the complex ribosomal association. Our results answer the fundamental question on how a paused ribosome resumes translation and show that Drg1/Dfrp1 proteins play a critical role in ensuring orderly translation.

38 **INTRODUCTION**

39 Maintaining protein homeostasis is essential for cell physiology, and this process,
40 undoubtedly, is closely related to the accuracy and efficiency of protein synthesis. Disrupting
41 intracellular homeostasis underlines a wide range of human diseases [1-3]. The central translation
42 apparatus, the ribosome, is a major target of control through its interactions with diverse
43 proteins[4-6]. One of those proteins, the conserved developmentally-regulated GTP-binding
44 proteins (Drg), plays important roles in embryonic development, cellular growth, differentiation,
45 and proliferation. Drg was originally identified to be highly expressed in neural precursor cells in
46 the developing mouse brain [7]. Shortly after its discovery, Drg mRNA and protein were found to
47 be widely expressed at variable levels in cultured cells, as well as other embryonic, postnatal,
48 and adult murine tissues [8]. The coding sequence of Drg proteins contains a G-motif common to
49 the GTPase superfamily [9,10]. A phylogenetic study revealed that eukaryotes typically contain two
50 Drg genes, Drg1 and Drg2, that have highly homologues amino acid sequences (**Supplemental**
51 **Figure 1**), whereas archaea contain only one [11].

52

53 In the cell, expression of Drg proteins is controlled by Drg family regulatory proteins
54 (Dfrp) through direct physical associations: Dfrp1 specifically binds Drg1, whereas Dfrp2 binds
55 to Drg2 preferentially [12]. Like the Drgs, the sequences of Dfrp proteins are highly conserved.
56 Yeast and mammalian Dfrp proteins share a partially-conserved sequence of about 60 amino
57 acids, the DFRP domain, which is critical for binding to Drg proteins (**Supplemental Figure 1).**
58 Importantly, association of Dfrp and Drg proteins confers stability to the Drg protein in vivo [12]
59 and enhances the GTPase activity of the Drg in vitro [13,14].

60

61 Both Drg and Dfrp proteins are conserved from yeast to human suggesting that they play
62 important functions in fundamental pathways in eukaryotic cells. These proteins are highly
63 expressed in actively growing and developing cells, as well as reproductive adult tissues of
64 plants, animals, and humans. Consistent with their functions in growth control, altered Drg
65 expression leads to cell transformation or cell cycle arrest [15-18]. While high levels of Drg
66 expression are positively correlated with their functions in translation, and both Drg1/Dfrp1 and
67 Drg2/Dfrp2 complexes copurify with translation factors [19], the role played by these proteins in
68 translation is not understood. Here, we report molecular functions of the yeast Drg1/Dfrp1
69 ortholog, Rbg1/Tma46, in translation and the structural basis of their mechanism of action on the
70 ribosome.
71
72
73 **RESULTS**
74 To effectively capture and compare *in vivo* ribosome dynamics in a drug-free way at a
75 genome-wide scale, we employed the 5PSeq method (**Supplemental Figure 2A and 2B**), which
76 captures 5' monophosphate (5P) mRNA intermediates, produced by 5' exonucleases (Xrn1 in
77 yeast) that follow the last translating ribosome on an mRNA [20]. As a result, 5PSeq enriches
78 ribosome footprints on the mRNA undergoing 5' to 3' co-translational degradation, providing a
79 sensitive measure of ribosome dynamics in translation and quality control pathways. Using this
80 technique, we observe large a degree of ribosome pauses on mRNAs, even in the wild-type cell,
81 showing that translation pause is likely to be ubiquitous in the cell.
82

83 In parallel, we created the Δrbg1 strain and multiple knockouts of genes functionally
84 related to Δrbg1. The obviously reduced fitness of yeast cells as a result of double mutants of the
85 Drg/Dfrp family members (Rbg1, Rbg2, Tma46, and Gir2) [21] suggests at least a partially-
86 overlapping functional consequence between the two Drg/Dfrp complexes. Furthermore, yeast
87 genetic screens followed by biochemical investigations showed that one of either the
88 Rbg1/Tma46 or Rbg2/Gir2 complexes was required for uncompromised growth of cells lacking
89 the slh1 gene [19]. The protein product of this gene, Slh1, is another highly conserved eukaryotic
90 protein that associates with ribosomes [19] and it is known to be important for the ribosome-
91 associated quality control (RQC) [22-26]. Simultaneous functional inactivation of Rbg1, Rbg2, and
92 Slh1 results in serious growth defects [19]. Therefore, we created a conditional triple-knockout
93 strain, Δrbg2Δslh1-Rbg1d, by simultaneously inhibiting Rbg1 mRNA transcription and
94 promoting Rbg1 protein degradation [27,28] . This way, when combined with the single (Δrbg1)
95 and double (Δrbg2Δslh1) knockouts, cellular functions of Rbg1 can be specifically examined and
96 the partially overlapping functions of the three proteins, Rbg1, Rbg2, and Slh1, can also be
97 studied (**Supplemental Figure 3A**).
98
99 Similar growth phenotype patterns were observed at 19, 30, and 37°C for the wild-type
100 and all mutant strains (**Supplemental Figure 3B**), suggesting the conditional knockout strain
101 Δrbg1Δslh1-Rbg1d works in the manner expected, and the cellular function of Rbg1 is
102 temperature-independent. Furthermore, a progressive decrease of the amount of polysomes and
103 increase in the amount of 40S, 60S, and 80S ribosomal fractions were observed when cells
104 depleted these three proteins one by one, demonstrating a gradual decrease of global translation
105 as cells are depleted of these three proteins one after another (**Supplemental Figure 3C**).

106

107 **1. Deletion of Rbg1 leads to accumulation of ribosomes at the start and stop codons.**

108 Using the 5P-Seq method, metagene analyses demonstrated progressively increasing peaks
109 at the -14 nt and 4 nt positions in Δrbg1, Δrbg2Δslh1 and Δrbg2Δslh1-Rbg1d cells (**Figure 1A**
110 **ii-iv**, solid lines in blue) when compared to the randomly fragmented mRNA control (dotted
111 lines in black) and the wild-type cells (**Figure 1A, i**). Since the length of ribosomal footprints
112 from the ribosomal P-site to its protected 5'-end is 14 nt in this experiment, these two positions
113 correspond to the ribosome pausing at the start codon and after seven amino acids have entered
114 the exit tunnel, respectively (**Supplemental Figure 4A and 4B)**.

115

116 At the stop codon, we also observe defects of slowed termination in Δrbg1 and
117 Δrbg2Δslh1-Rbg1d cells (**Figure 1B** and **Supplemental Figure 4C** and **4D**). In-line with the
118 function of Slh1, Δrbg2Δslh1 only shows a modest defect, suggesting that elongation stalling
119 resolved by Slh1 likely alleviates ribosome accumulation at the stop codon. In addition, we
120 found that ribosome pausing at the seventh amino acid was specifically associated with peptides
121 containing a MSxxxxx pattern (**Supplemental Figure 4E**) [20]. Other than this, no consensus
122 sequences at the amino acid or nucleotide levels were found at either the start or stop codons, nor
123 was any evidence found that specific cellular pathways are targeted by this phenomenon (data
124 not shown). These results show that functions of Rbg1 and Rbg2 are not likely limited to a
125 specialized pathway.

126

127 **2. Inactivation of Rbg1, Rbg2 and Slh1 results in redistribution and accumulation of**
128 **ribosomes in the 5' end of mRNA.**

129 The mRNA degradation machinery closely follows the last translating ribosome in
130 5PSeq, where the translation rate of the last ribosome affects the amount of 5P intermediates and
131 their positions in the coding region of mRNA. As a result, a 3-nt periodicity pattern of the 5P
132 intermediates in the coding region (CDS) informs about ribosome dynamics, where a strong 3-nt
133 periodicity is suggestive of slow translation, and weak 3-nt periodicity indicate fast (**Figure 1C**
134 **i)**. It has been suggested that in wild type cells, it's difficult for the exonuclease to catch up to the
135 last translating ribosome near the start codon because decapping was rate-limiting [20]. Compared
136 to those in the wild type, in Δrbg1, and Δrbg2Δslh1 cells, we observe a much clearer 3-nt
137 periodicity pattern of the 5P intermediates in the 5' end of coding regions in Δrbg2Δslh1-Rbg1d
138 cells (**Figure 1A and 1C-i**), suggesting that the rate of translation elongation was significantly
139 decreased when the cells lost the functions of Rbg1, Rbg2, and Slh1 simultaneously.
140
141 To characterize this phenomenon more quantitatively, we calculated the proportion of 5P
142 reads in the ribosome-protected frame for each codon. The proportion score for a control sample,
143 lacking the characteristic 3-nt periodicity pattern, was estimated to be around 0.33. In agreement
144 with an earlier observation [20], the proportion scores of 5P reads slowly increase from ~0.33 at the
145 start codon to ~0.45 at the 300nt position in the ribosome-protected frame for the wild type cells
146 (**Figure 1C ii-iv, black lines**). In contrast, the proportion values at the same position of the
147 mRNA increase noticeably faster in the Δrbg1 (red line in **Figure 1C ii**) and Δrbg2Δslh1 cells
148 (green line in **Figure 1C, iii**). However, this value increases to 0.45 immediately after the start
149 codon in the Δrbg2Δslh1-Rbg1d cells (blue line in **Figure 1C iv**), indicative of a substantial
150 decrease in the rate of elongation in these cells.
151

152 **3. Rbg1 alleviates ribosome pausing at specific amino acids and mRNA regions.**

153 Seemingly stochastic yet pervasive ribosome pauses were seen at the individual gene
154 level in our data. However, at the metagene level, we observed that ribosome pausing is
155 correlated with the translation of glutamic acids, aspartic acids, arginine and lysine (**Figure 2A**),
156 as well as serine and glycine but to a lesser degree. Considering that the length of ribosomal
157 footprints from the ribosomal A, P, and E-sites to its protected 5'-end is 17nt, 14 nt, and 11nt in
158 the 5P-Seq experiment (**Supplementary Figure 4A and 4C**), the observed pause in the
159 ribosome at the metagene level likely occurs at the amino acid instead of nucleotide level.

160

161 In agreement with the results at the start and stop codons, no specific cellular pathway is
162 targeted by Rbg1 proteins, which suggests that they play a general role in suppressing translation
163 pause. Heterogeneity of the peptide sequences is the hallmark of the translation pause observed
164 in our genomic data. Nevertheless, when we calculated the pause score at each position as
165 described with modifications [29], R/K-rich sequences stood out as one common feature in all
166 Δrbg1, Δrbg2Δslh1 and Δrbg2Δslh1-Rbg1d (**Figure 2B**). This result correlates well with the
167 strong pausing effects of these two amino acids in the ribosome, and enrichment analysis was
168 carried out on the most affected R/K-rich mRNA transcripts when Rbg1, Rbg2 and Slh1 are
169 absent (**Supplemental Figure 5**).

170

171 The conclusions drawn from the genomic investigations described above were tested by
172 comparing the rate at which wild type cells grow in the presence of anisomycin to the rate at
173 which cells lacking Rbg1 grow under the same conditions. The antibiotic anisomycin is known
174 to cause translational stalling by binding to the peptidyl transferase center (PTC) of the ribosome

175 [30]. In the presence of 10 μg/ml anisomycin, the Rbg1 deletion strain grows slightly, but
176 observably slower on YEPD plates than wild type yeast cells (**Figure 3A,** the second line of cell
177 growth), but this growth defect is revered when Rbg1 proteins is expressed in Δrbg1 cells
178 (**Figure 3A,** the third line of cell growth).
179
180 To find out if Rbg1 facilitates the translation stalling on mRNA and protects mRNA
181 harboring stalling signals from degradation that results from mRNA surveillance, we
182 transformed cells with a construct mRNA containing twelve consecutive Arginine codons (R_{12}),
183 a sequence known to trigger mRNA no-go decay [24,31], and monitor the degree of its translation
184 using flow cytometry. Based on the experimental design (**Figure 3B, i)**, the intensity of the GFP
185 fluorescence in counted cell populations is an indicator of the translation and the degree of
186 stability of the construct mRNA. Compared to the WT cells (**Figure 3B, ii)**, deletion of Rbg1 in
187 the cell results in an increased number of cells with no GFP fluorescence (**Figure 3B, iii**),
188 suggesting an increased degree of mRNA degradation. In contrast, the presence of Rbg1 in the
189 Δrbg2Δslh1 cells leads to much enhanced GFP fluorescence, compared to not only the ΔRbg1
190 cells, but also wild type cells. This result shows that Rbg1 indeed enhances the mRNA
191 translation, stabilizes the mRNA and prevents them from undergoing no-go decay (**Figure 3B,**
192 **iv)**.
193
194 **4. Structural basis of enhanced translation by heterodimeric GTPase Rbg1/Tma46 binding**
195 **to the ribosome**
196 To gain insights into molecular interactions important for the heterodimeric GTPase's
197 function, we obtained a cryoEM structure of the ribosome with Rbg1/Tma46 bound**.** A TAP tag

198 was inserted at the end of the yeast chromosomal Rbg1 gene and the native Rbg1/Tma46-
199 ribosomal complexes were purified from cellular ribosomal fractions using affinity pulldown.
200 This method allows us to comprehensively sample physiologically-relevant functional states of
201 the ribosome when the protein heterodimer binds. A more detailed experimental procedure is
202 outlined in **Supplemental Figure 6**.
203
204 As shown in **Figure 4A**, we captured ribosomes in the classical ligand binding state with
205 two tRNAs in the ribosomal A and P sites, protein eIF5A[28,32,33] in the E-site and Rbg1/Tma46
206 bound to the GTPase association center (GAC). The ribosomes are in the translational state that
207 they assume after peptide bond formation has occur but before tRNA translocation has taken
208 place, with the nascent peptides attached to the CCA-end of the tRNA in the ribosomal A site.
209
210 The HTH (helix-turn-helix) and G domain of Rbg1 bind to the 60S subunit, with
211 conserved residues in the α4 helix of Rbg1 interacting with the sarcin-ricin loop of the GAC
212 (**Figure 4B**). Compared with the crystal structure of Rbg1/Tma46 (**Supplemental Figure 7**) in
213 isolation, S5D2L (S5 Domain 2 Like) domain of Rbg1 extends out and charges residues in the
214 loop regions between β6 and β7, as well as α6 and β8 interacts with A-tRNA (**Figure 4C**), and
215 the TGS domain rotates ~17 degrees and binds to h5 of the 18S rRNA (**Figure 4D**). These
216 interactions are conserved (**Supplemental Figure 8**), suggesting that they are functionally
217 important. Earlier studies showed that deletion of the TGS domain in Rbg1, or mutations in
218 Rbg1's G domain which either compromise the nucleotide-binding or GTPase activities of the
219 protein, failed to rescue the severe growth defect in the triple knockout Δrbg1Δrbg2Δslh1 cell [19].
220

221 Tma46 adopts an extended structure and wraps around Rbg1. Their interaction is
222 stabilized by extensive highly conserved hydrophobic contact. The second zinc-finger at the N-
223 terminal region of Tma46 is ordered and binds to the gap formed between h16 and h33 of the
224 40S head and shoulder domains, respectively, establishing an interaction unique to the
225 heterodimeric GTPase that is absent from other known monomeric translational GTPases such as
226 EF-Tu, EF-G, RF3 (**Figure 4E**). This interaction is critical for mediating the ribosomal
227 association of the heterodimeric GTPase. As shown in **Figure 4F**, deletion of the N-terminal
228 Zinc-finger domain of Tma46 completely abolishes binding of Rbg1/Tma46 to the ribosome,
229 regardless of whether Rbg1 is in the GDP or GTP-bound states. This result demonstrates that the
230 zinc-finger domain of Tma46, while not required for Rbg1/Tma46 heterodimer formation [13], is
231 required for ribosomal association.
232
233
234 **DISCUSSIONS**

235 Translation proceeds at a non-uniform rate, with ribosomes pause as they progress down
236 coding sequences on mRNA. As data demonstrated in this investigation, the ribosome pauses at
237 every codon it encounters to execute the steps of the translation cycle, and that pausing is
238 responsible for the 3-nt periodicity in the 5P-Seq. The pauses that occur at start and stop codons
239 are longer than those seen in the elongation cycle because of the complexity of the events
240 associated with initiation and termination. In the middle of coding sequences, variations in
241 concentrations of cognate tRNAs as well as elongation factors play an important role in
242 determining the rates at which particular codons are translated. Besides the "normal" pause, a
243 prolonged pause of the ribosome could have effects ranging from "impediment but

244 inconsequential" to detrimental, such as a translation arrest due to mRNA secondary structural
245 elements, specific peptide motifs or damages in the mRNA [34-38]. How ribosomes that have
246 paused during the translation of a particular codon for a time longer than usual are recognized
247 and targeted so that protein synthesis can continue is an important question. In this study, we
248 show that in eukaryotes, conserved Drg proteins and their partners, Dfrps, play an important role
249 in this process. The genomic experiments reported above show that the yeast ortholog of
250 Drg1/Dfrp1, Rbg1/Tma46, reduces the pausing seen during initiation and termination, and
251 enhances the overall rate of elongation. It is possible that the observed initiation arrest and
252 elongation rate decline in all mutant strains, Δrbg1, Δrbg2Δslh1 and Δrbg2Δslh1-Rbg1d, are
253 coupled. Remarkably, these negative impacts are accumulative, with the mildest defect occurring
254 in the single knockout and the most severe defect occurring in the Δrbg2Δslh1-Rbg1d cell.
255 Subsequent analysis indicates accumulated ribosome pauses underlines the observed
256 phenomenon.

257

258 **Proposed Mechanism of Action:** Our single-particle cryoEM reconstruction shows that
259 the Rbg1/Tma46 complex targets translating ribosomes after peptide-bond formation has taken
260 place, but before tRNA translocation. How does Rbg1/Tma46 promote efficient translation? In
261 contrast to the altered conformations reported when stalling peptides reside in the exit tunnel
262 without the Rbg1/Tma46 complex [39-41], the ribosomal decoding and peptidyl transferase centers
263 assume conformations similar to what is observed in ribosomes competent to proceed further in
264 the elongation cycle when Rbg1/Tma46 binds. This suggests that Rbg1/Tma46 acts by
265 stabilizing pausing ribosomes in a productive conformation. Since this GTPase binds to the state
266 immediately after peptide-bond formation, with the nascent peptide attached to the CCA-end of

267 the A-tRNAs, it's possible that binding of Rbg1/Tma46 facilitates tRNA interactions and peptide
268 bond formation in the ribosome.
269
270 It is worth mentioning that the sheer number of ribosomal pause sites detected by the
271 5PSeq experiment, even in the wild-type cells, and the heterogeneity of the pausing sequences
272 are striking to us, showing that translation pause is indeed a widespread phenomenon in
273 eukaryotic cells. This phenomenon was also observed in several earlier studies [28,33,42] . Then,
274 *how does Rbg1/Tma46 promote efficient translation in such a diverse molecular environment?*
275
276 Unlike other known monomeric translational GTPases, the heterodimeric GTPase
277 Rbg1/Tma46 binds to the ribosome in both the GTP- and GDP-bound states in vitro (**Figure 4F**),
278 indicating that it plays somewhat related, yet distinctive functions in translation. It's reasonable
279 to think that when translation pauses, E-tRNA leaves and vacates the ribosomal E-site. The zinc
280 finger in the Tma46-subunit senses the movements in the 40S and binds to the gap between the
281 head and shoulder domain. Stabilized by the Tma46-40S interaction, the nucleotide binding and
282 GTP hydrolysis in the Rbg1-subunit might help the ribosome and tRNAs to navigate through a
283 range of conformational and energetic landscapes resulted from heterogeneous pause signals,
284 thereby achieving an efficient peptide-bond formation. Indeed, Nucleotide binding and GTP
285 hydrolysis are important for both Rbg1's association with the ribosome and its cellular
286 functions[19]. In addition, Rbg1/Tma46 has a relatively low intrinsic nucleotide-binding and GTP-
287 hydrolysis activity, this property may help the replacement of this GTPase by other elongation
288 factors once their task is accomplished in the ribosome.
289

290 Because of the conserved nature of Rbg1/Tma46, a similar function is likely to be
291 observed in higher eukaryotic organisms. Furthermore, the amino acid sequences of Drg1 and
292 Drg2 are highly homologous with each other. Importantly, residues in Rbg1 that interact with
293 the ribosome and tRNAs are either conserved or highly homologous, not only within the Drg1
294 family of proteins, but also between Drg1 and Drg2. This suggests that the Drg2 protein likely
295 interacts with the translating ribosomes in a similar way and facilitates translation in a similar
296 manner.
297
298 In contrast, amino acid sequences of Dfrp1 and Dfrp2, the Drg family regulatory proteins,
299 are quite different except for their DFRP domain (**Supplemental Figure 1**). This suggests that
300 the two Dfrp proteins are involved in different protein-protein interactions to engage Drg
301 proteins to the ribosome, as also seen in yeast colliding ribosomes involve Gcn1 [43]. Our structure
302 explains earlier experimental observations that Dfrp1 specifically binds Drg1, and Dfrp2 binds to
303 Drg2 preferentially [12]. As seen in the structure, molecular interactions between Rbg1 and Tma46
304 are largely hydrophobic (**Supplemental Figure 1 and 8**). However, Rbg2 does not process the
305 same amino acids with hydrophobic sidechains at the protein interface as Rbg1 does
306 (**Supplemental Figure 8**), this molecular difference explains why Tma46 and Rbg2 does not
307 bind together. On the other hand, some hydrophobic residues in Tma46 are conserved in Gir2,
308 which has residues that could potentially interact with Rbg1 via other interactions at the protein
309 interface, for example by formation of hydrogen bonds. Nevertheless, the weak cross-
310 association of Drg1 and Dfrp2 [44] in the otherwise specific and distinct complexes, rules out the
311 strict exclusiveness of the two Drg/Dfrp classes and suggests another fine-tuned layer of control
312 in the cell.

313

314 Furthermore, while two Drg proteins likely play the same function on the ribosome, they
315 are obviously involved in different translational events due to their distinctive Dfrp partners.
316 Based on the data from flow cytometry (**Figure 3B**) where Rbg1 in the ΔRbg2ΔSlh1 leads to
317 stronger GFP signal produced from translation of mRNA with stalling sequences compared to
318 the WT cells, Drg1 likely plays a more general role than Drg2 in the cell.

319

320 It came as a pleasant surprise that a general translation factor eIF5A was seen in the
321 Rbg1/Tma46-bound ribosomal complex we studied. This protein is known to bind to the
322 ribosomal E site [45,46] and associates with the ribosome when translation stalls [47,48]. Translation at
323 proline stretches is facilitated by eIF5A [32]. While we indeed observe strong pause of ribosome
324 when translating proline in wild type cells, deletion of Rbg1 does not exacerbate this effect (data
325 not shown), suggesting mechanisms by which eIF5A and Rbg1/Tma46 promote translation likely
326 to be different.

327

328 Translation pause can be viewed as a two-sided event: from the point of view of protein
329 synthesis, a pause needs to be suppressed so that the protein synthesis can be resumed, and a
330 protein can be made efficiently. However, on the other hand, a pause also provides a valuable
331 chance for regulation. Whether Drg1/Dfrp1 acts as a suppressor of ribosome pausing at sites
332 where mistakes (or suboptimal peptide bond formation) can occur is an important question for
333 future study.

334

335 **Functional interplay of Drg1/Dfrp1, Drg2/Dfrp2 and ASCC3** The cumulative effects
336 observed in this study among Δrbg1, Δrbg2Δslh1, and Δrbg2Δslh1-Rbg1d cells strongly suggest
337 shared functions for Drg/Dfrp and ASCC3 (the mammalian counterpart of Slh1) proteins in
338 fundamental biological processes. While it is still possible that the direct cellular targets and
339 molecular functions of these proteins may not be the same, evidence available shows that the
340 ribosome is one of their shared targets. Here, we propose these three proteins help to ensure
341 cellular protein homeostasis by targeting ribosomes involved at the junction of protein synthesis
342 and quality control pathways (**Figure 5**). When translation pauses, the Drg/Dfrp protein helps
343 ribosomes to navigate through and find its way to pass the pause, thereby allowing the ribosomes
344 behind it in the queue to continue using the mRNA as a template for protein synthesis. In the
345 absence of Drg/Dfrp, ASCC3 likely guides the paused ribosome to the quality control pathway.
346 Since the exact role of ASCC3 in the RQC or NGD is unclear, more investigations will be
347 needed to reveal details at the molecular level.
348
349 Whether Rbg1/Tma46 participates in ribosomal subunit disassociation is an important
350 question to answer in future investigations. In addition, we found that it hydrolyzes ATP five
351 times faster than GTP in vitro (Jin lab, unpublished data). It remains to be seen if association of
352 this protein complex with the ribosome helps to couple metabolic and energetic state of the cell
353 with efficient protein synthesis.
354
355 As a final note, Drg proteins play important roles in some cellular processes that appear
356 to be unrelated to translation. For example, they are involved in spindle checkpoint signaling,
357 and elevated levels of Drg1 protein causes lung adenocarcinoma and taxol resistance [49]. In an *in*

358 *vitro* study, Drg1 was reported to diffuse on microtubules, to promote microtubule
359 polymerization, and to drive microtubule bundle formation in a GTP-independent manner [50].
360 Additionally, HeLa cells with reduced Drg1 levels show delayed progression from prophase to
361 anaphase due to a slowed spindle formation [50]. Further investigations are required to see if these
362 seemingly unrelated processes crosstalk with translation.
363
364 Maintaining protein homeostasis during critical stages and conditions such as
365 development, proliferation, and cellular stress conditions is critical for eukaryotic organisms. It is
366 not surprising that the translational machinery is one of the major targets of regulation for this
367 purpose. Our observations provide links between translation pause and protein quality control, a
368 critical component in maintaining protein homeostasis and cell physiology. It is worth
369 mentioning that other pathways may crosstalk with these processes to achieve the same goal.
370

371

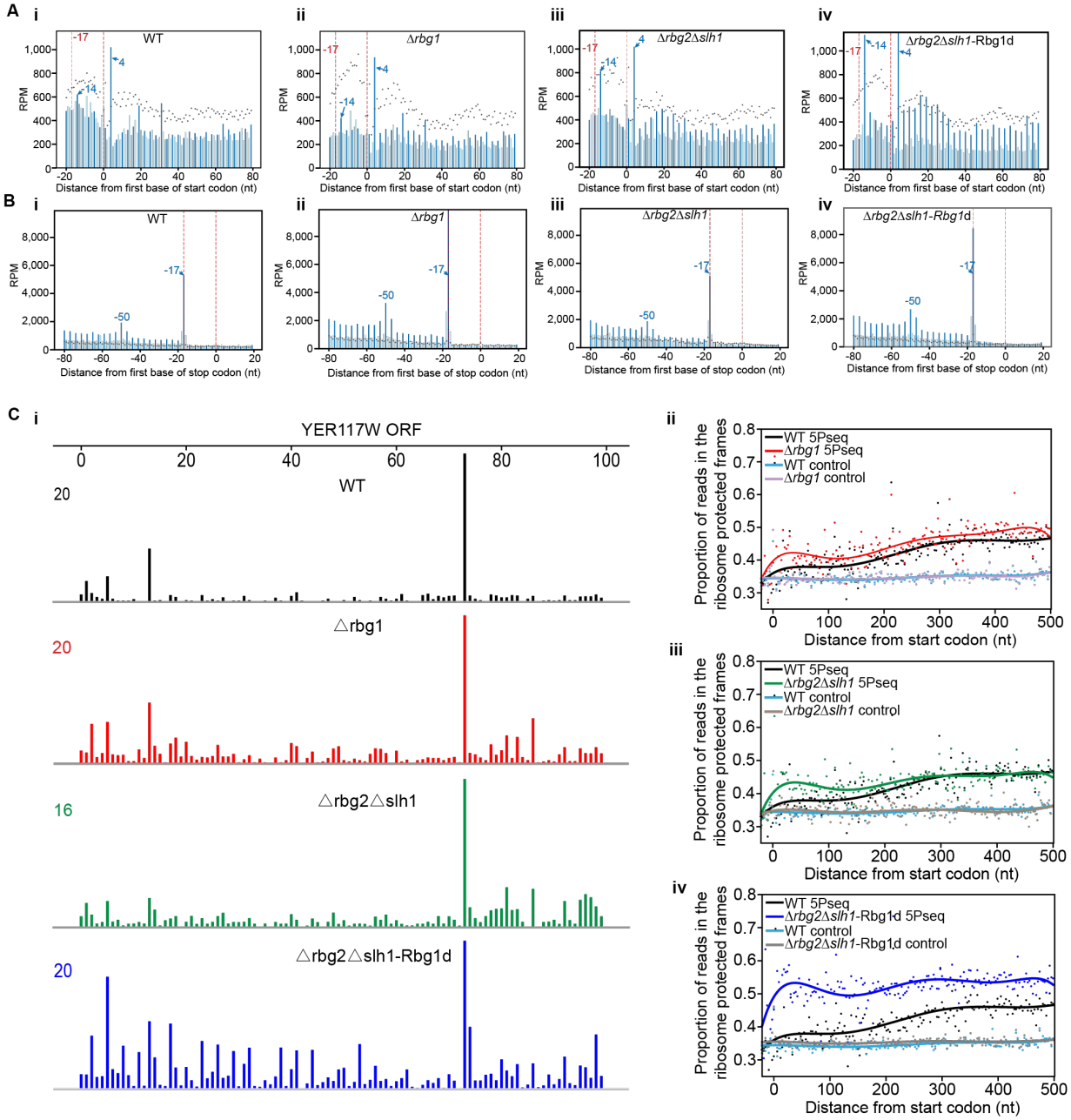

372

373

374

375 **Figure 1. Deletion of Rbg1 results in slow translation initiation, elongation and termination**

376 **A. Translation initiation arrests in mutant cells.** Normal translation pauses at start codons in

377 wild type cells; and increased ribosome pauses at start codons in Δrbg1, Δrbg2Δslh1, and

378 Δrbg2Δslh1-Rbg1d cells. Metagene analysis displaying the abundance of 5'P reads relative to
379 start codons for WT, Δ*rbg1*, Δ*rbg2*Δ*slh1* and Δ*rbg2*Δ*slh1*-Rbg1d strains, or after random
380 fragmentation (5PSeq control, dotted black line). Reads are represented by RPM, with the blue
381 bar indicating the +1 frame and light blue bars indicating the 0 and +2 frames. The two dotted
382 red lines show the positions of 0 and -17nt relative to the start codon. The blue peak at -14nt
383 corresponds to the protected region from a putative initiation-paused ribosome and the peak at
384 4nt is caused by peptide-induced ribosomal arrest. Biological replicates are averaged.
385 **B**. **Effects on translation termination in mutant cells.** Normal translation pauses at stop
386 codons in wild type cells and altered pauses in the three mutants Δrbg1, Δrbg2Δslh1, and
387 Δrbg2Δslh1-Rbg1d. Peaks at the -17nt position denote ribosomes with a stop codon in the A site;
388 and the pause at the -50nt position is indicative of a disome position, with the leading ribosome
389 reaching translation termination. Other experimental details are the same as described in **A**.
390 **C. Slower translational elongation after depletion of Rbg1, Rbg2, and Slh1. i**.
391 Representative genome tracks of the 5' ends of 5PSeq reads in WT (black), Δ*rbg1* (red),
392 Δ*rbg2*Δ*slh1* (green), and Δ*rbg2*Δ*slh1*-Rbg1d strains (blue). Coverage is expressed in RPM. An
393 obvious 3-nt periodicity pattern was observed for YER177W mRNA in the Δrbg2Δslh1-Rbg1d
394 strain. **ii-iv:** The proportion of 5PSeq reads in the ribosome-protected frame (Frame 1 in
395 **Supplementary Figure 2**) shows that the 5' end of mRNA was protected by ribosomes in the
396 Δrbg2Δslh1-Rbg1d strain. Proportion scores were calculated for each codon by normalizing the
397 read counts in frame 1 to the total reads in all three frames within the same codon. These are
398 shown as dots with smoothed lines (polynomial fitting) for genes longer than 1000 base pairs
399 (bp) and with RPKM values > 20. Only the region containing -20 nt to 501 nt with respect to the
400 first base of start codon were used to calculate the proportion score. 5Pseq samples from Δ*rbg1*

401 (ii, red), Δ*rbg2*Δ*slh1* (iii, green), and Δ*rbg2*Δ*slh1*-Rbg1d (iv, blue) strains were compared to WT

402 strains (black). Random fragmentation samples (control) are also shown. Biological replicates

403 are averaged.

404

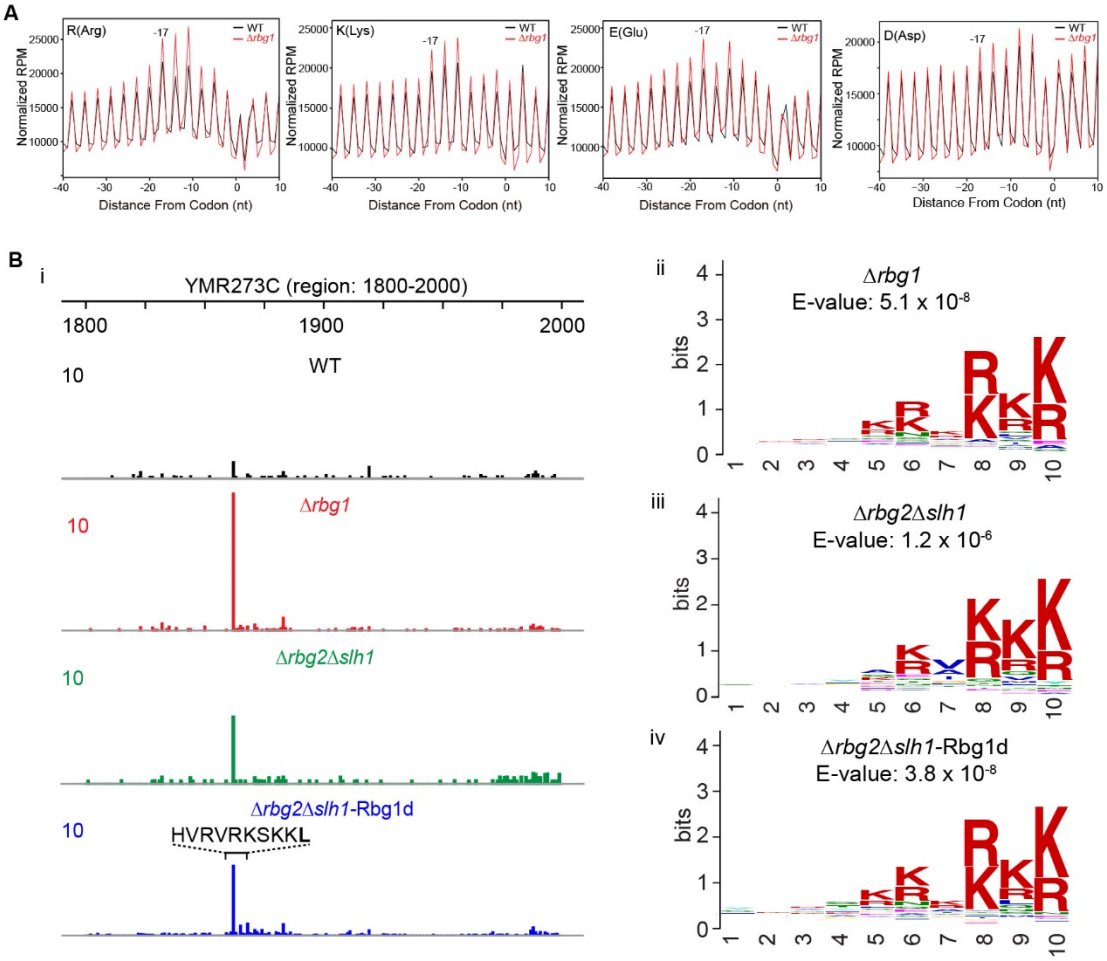

Figure 2. Rbg1 suppresses ribosome pause in translation.

A. Increased translation pauses at Arg, Lys, Glu and Asp positions in the absence of Rbg1. The metagene (-40 to +10 window) which shows the number of 5P intermediates from translation of Arg, Lys, Glu and Asp amino acids and their ribosomal positions in ΔRbg1 (red lines) and WT (black lines) cells. The total number of reads was normalized to facilitate data analysis and comparison, and data were analyzed as described [33]. The -17nt, -14nt and -11nt peaks represent indicated codons at the ribosomal A, P and E sites, respectively.

B. Rbg1 alleviates ribosome pausing at arginine/lysine-rich regions. i. Representative genome tracks of 5' ends of 5PSeq reads. Genome tracks of the 5' ends of 5PSeq reads in WT (black), Δ*rbg1* (red), Δ*rbg2*Δ*slh1* (green), and Δ*rbg2*Δ*slh1*-Rbg1d (blue) strains were shown

416 around the arginine-/lysine-rich region. Coverage is expressed in average RPM of the biological
417 duplicates. **ii-iv. Translation pauses at the R-/K-rich region in Δ*rbg1*, Δ*rbg2*Δ*slh1*, and**
418 **Δ*rbg2*Δ*slh1*-Rbg1d strains.** To identify specific peptide sequences which induce ribosome
419 pausing while being translated in the knockout strains, pause scores were first calculated by
420 dividing the RPM value at each position of the transcript by the mean RPM value for the ten
421 codons upstream and downstream of the same position. The ten amino acids upstream with a
422 pause score > 10 were compared to those with pause scores < 10 using MEME [51]. Amino acid
423 sequences extracted from the WT strain show no consensus sequence.
424

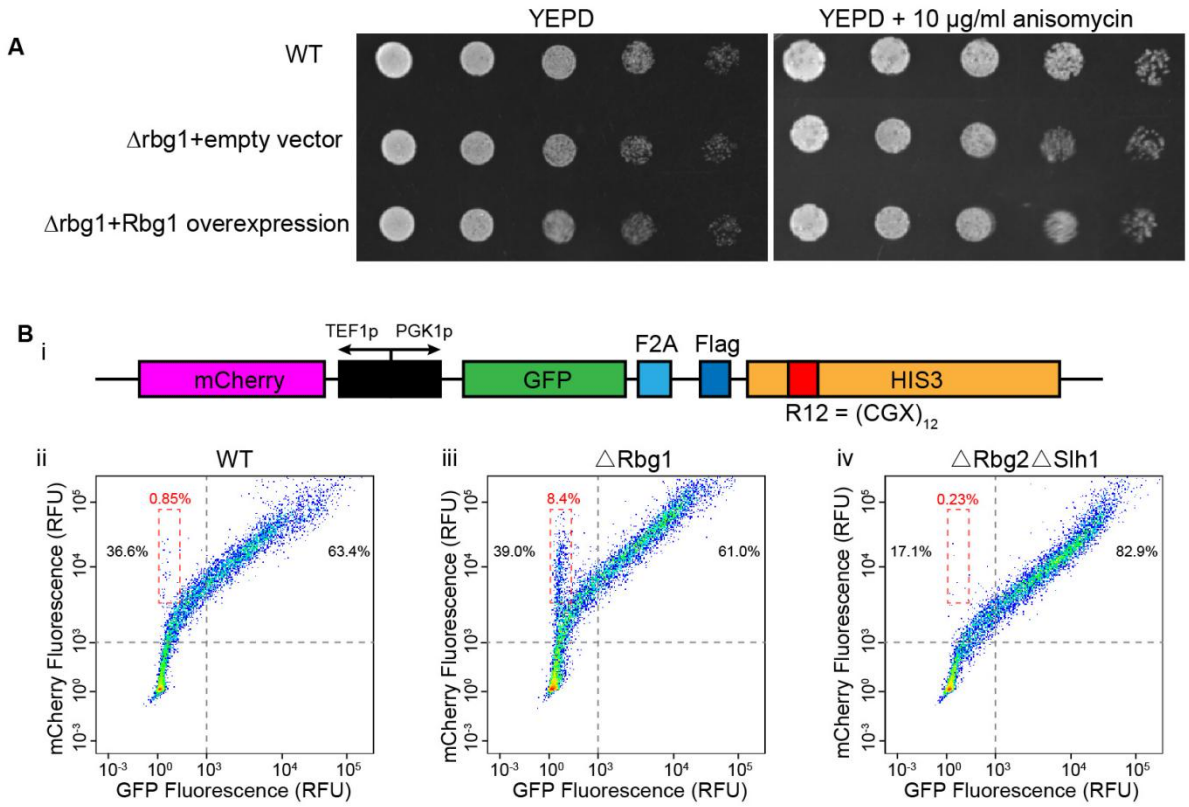

Figure 3. Rbg1 promotes efficient translation.

A. Deletion of Rbg1 results in slower growth for yeast cells in the presence of anisomycin. Expression of Rbg1 protein in the Δrbg1 cells restored growth. Δrbg1 cells were transformed with either an empty vector, or a vector containing the rbg1 gene with a PGK1 promoter. Serial dilutions of exponential phase liquid cultures were spotted on YEPD, with or without 10 µg/ml anisomycin, and were incubated at 30 ˚C for 2 days.

B. Rbg1 enhances translation of mRNAs harboring an intrinsic stalling sequence. Yeast cells expressing the indicated mRNA with the R12 sequence, fluorescent mCherry and GFP reporters (top panel) were grown to exponential phase (OD_{600}=0.6) and were analyzed by flow cytometry. mCherry and GFP fluorescence intensities in the cell were monitored simultaneously using 561 nm and 488 nm excitation lasers, respectively. Scatterplots of 10,000 individual cells of the WT, Δrbg1 and Δrbg2Δslh1 background are displayed separately. The scatterplots are

438 shown on a bi-exponential scale with pseudo-color in order to better visualize data across the
439 wide range of expression levels seen in these experiments. According to the control cells which
440 do not express the indicated mRNA construct (data not shown), only the cells with more than 10^3
441 relative fluorescence unit (RFU) of mCherry fluorescence are considered to contain enough
442 mRNAs and are subjected to further analysis. WT, Δrbg1 and Δrbg2Δslh1 cells with $>10^3$ RFU
443 mCherry intensities are divided into two groups, shown as percentages in grey dashed lines.
444 Cells in the dashed box have high mCherry expression levels, but low GFP expression levels, the
445 amount of which in WT, ΔRbg1, ΔRbg1ΔSlh1 is shown accordingly as percentages (red) (ii, iii
446 and iv). The relative cell quantities at each position are indicated using a red to blue spectrum,
447 where the red color represents the largest cell population, blue represents the smallest one.
448
449

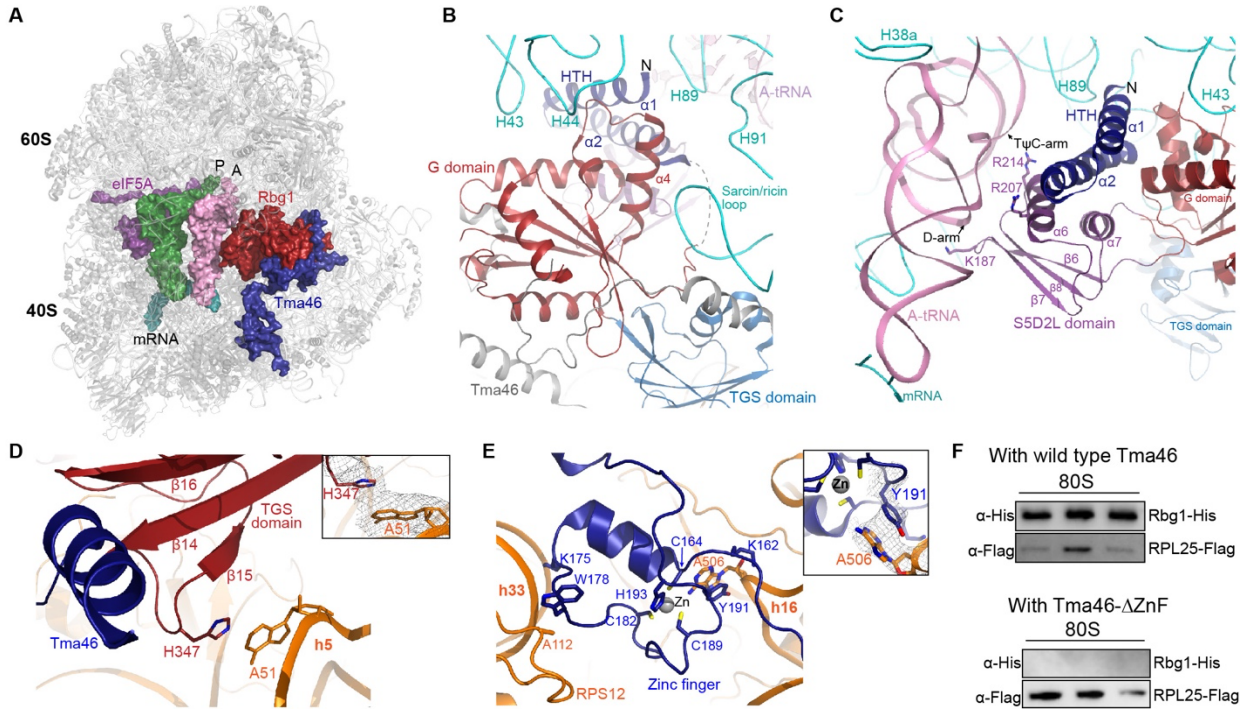

Figure 4. Structural basis for an enhanced translation when Rbg1/Tam46 binds to a paused ribosome.

A An **o**verall structure of Rbg1/Tma46-bound ribosomes. The ribosome is colored in grey. P-tRNAs, A-tRNAs-nascent peptides, eIF5A, Rbg1 and Tma46 are colored in green, pink, magenta, red and blue, respectively. Detailed essential interactions of the Rbg1 G domain with the sarcin-ricin loop (**B**), S5D2L domain with A-tRNA (**C**), TGS domain with the h5 in the 40S subunit (**D**), and the second zinc finger in Tma46 with the head and shoulder regions of the 40S subunit (**E**).

F. The Rbg1/Tma46 complex binds to the ribosome via the zinc-finger domain of Tma46. Proteins co-expressed in the *E.coli* BL21 strain were purified and incubated with pure 80S ribosomes, then ribosomal complexes were separated by sedimentation through a 10-50% sucrose gradient. Binding of Rbg1/Tma46 to the ribosome was determined by western blot. Flag-

464 tagged RPL25 was immunoblotted on the same membrane. Both the GTP- and GDP-bound

465 heterodimeric GTPases bound to the 80S ribosome, but only the GTP-bound state is shown.

466

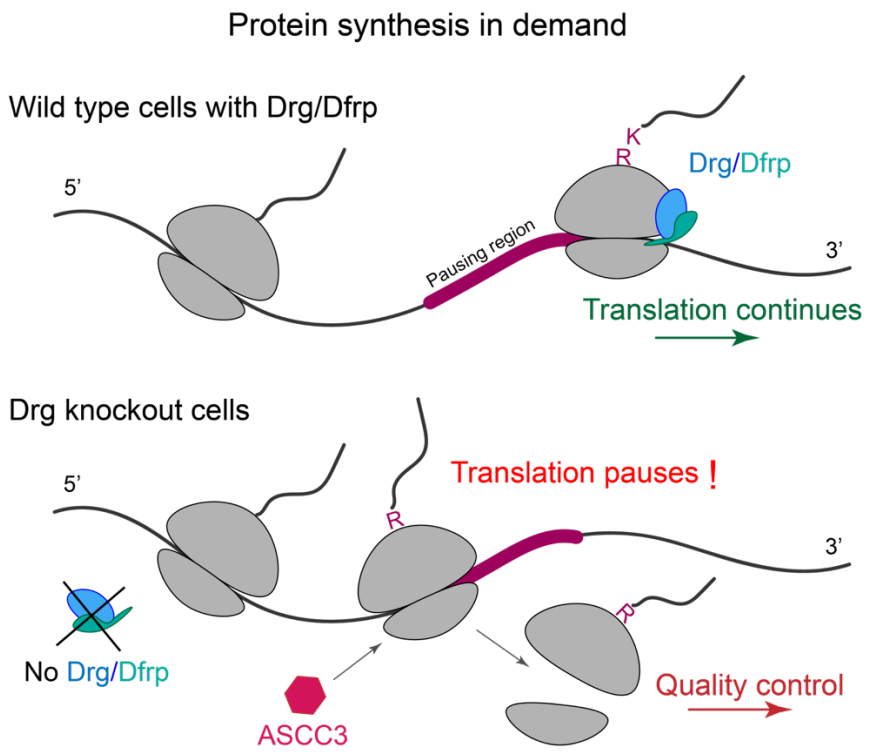

467

468

469 **Figure 5. Functional interplay of Drg/Dfrp and ASCC in the translation pause-and-resume**

470 **and quality control pathways.**

471 When translation pauses, Drg/Dfrp senses the paused ribosome and uses GTP-hydrolysis in the

472 Drg subunit to promote efficient translation, whereby allowing subsequent ribosomes to continue

473 translating the mRNA. In the absence of Drg/Dfrp, another protein called ASCC3, binds the

474 stalled ribosome and triggers subunit disassociation, followed by mRNA degradation and no-go

475 decay.

476

477

478 References Cited

479

480 1. Balchin, D., Hayer-Hartl, M. & Hartl, F.U. In vivo aspects of protein folding and quality
481 control. *Science* **353**, aac4354 (2016).

482 2. Labbadia, J. & Morimoto, R.I. The biology of proteostasis in aging and disease. *Annu Rev*
483 *Biochem* **84**, 435-64 (2015).

484 3. Wolff, S., Weissman, J.S. & Dillin, A. Differential scales of protein quality control. *Cell*
485 **157**, 52-64 (2014).

486 4. D'Orazio, K.N. & Green, R. Ribosome states signal RNA quality control. *Mol Cell* (2021).

487 5. Joazeiro, C.A.P. Mechanisms and functions of ribosome-associated protein quality
488 control. *Nat Rev Mol Cell Biol* (2019).

489 6. Brandman, O. & Hegde, R.S. Ribosome-associated protein quality control. *Nat Struct Mol*
490 *Biol* **23**, 7-15 (2016).

491 7. Kumar, S., Tomooka, Y. & Noda, M. Identification of a set of genes with developmentally
492 down-regulated expression in the mouse brain. *Biochem Biophys Res Commun* **185**,
493 1155-61 (1992).

494 8. Sazuka, T. et al. Expression of DRG during murine embryonic development. *Biochem*
495 *Biophys Res Commun* **189**, 371-7 (1992).

496 9. Leipe, D.D., Wolf, Y.I., Koonin, E.V. & Aravind, L. Classification and evolution of P-loop
497 GTPases and related ATPases. *J Mol Biol* **317**, 41-72 (2002).

498 10. Sazuka, T., Tomooka, Y., Ikawa, Y., Noda, M. & Kumar, S. DRG: a novel developmentally
499 regulated GTP-binding protein. *Biochem Biophys Res Commun* **189**, 363-70 (1992).

500 11. Li, B. & Trueb, B. DRG represents a family of two closely related GTP-binding proteins.
501 *Biochim Biophys Acta* **1491**, 196-204 (2000).

502 12. Ishikawa, K., Azuma, S., Ikawa, S., Semba, K. & Inoue, J. Identification of DRG family
503 regulatory proteins (DFRPs): specific regulation of DRG1 and DRG2. *Genes Cells* **10**, 139-
504 50 (2005).

505 13. Francis, S.M., Gas, M.E., Daugeron, M.C., Bravo, J. & Seraphin, B. Rbg1-Tma46 dimer
506 structure reveals new functional domains and their role in polysome recruitment.
507 *Nucleic Acids Res* **40**, 11100-14 (2012).

508 14. O'Connell, A., Robin, G., Kobe, B. & Botella, J.R. Biochemical characterization of
509 Arabidopsis developmentally regulated G-proteins (DRGs). *Protein Expr Purif* **67**, 88-95
510 (2009).

511 15. Song, H. et al. Overexpression of DRG2 Increases G2/M Phase Cells and Decreases
512 Sensitivity to Nocodazole-Induced Apoptosis. *The Journal of Biochemistry* **135**, 331-335
513 (2004).

514 16. Mahajan, M.A., Park, S.T. & Sun, X.H. Association of a novel GTP binding protein, DRG,
515 with TAL oncogenic proteins. *Oncogene* **12**, 2343-50 (1996).

516 17. Zhao, X.-F. & Aplan, P.D. SCL binds the human homologue of DRG in vivo1The DRG cDNA
517 sequence has been deposited in GenBank under accession number AF078103.1.
518 *Biochimica et Biophysica Acta (BBA) - Molecular Cell Research* **1448**, 109-114 (1998).

519 18. Schenker, T., Lach, C., Kessler, B., Calderara, S. & Trueb, B. A novel GTP-binding protein
520 which is selectively repressed in SV40 transformed fibroblasts. *J Biol Chem* **269**, 25447-
521 53 (1994).

522 19. Daugeron, M.C., Prouteau, M., Lacroute, F. & Seraphin, B. The highly conserved
523 eukaryotic DRG factors are required for efficient translation in a manner redundant with
524 the putative RNA helicase Slh1. *Nucleic Acids Res* **39**, 2221-33 (2011).

525 20. Pelechano, V., Wei, W. & Steinmetz, L.M. Widespread Co-translational RNA Decay
526 Reveals Ribosome Dynamics. *Cell* **161**, 1400-12 (2015).

527 21. Decourty, L. et al. Linking functionally related genes by sensitive and quantitative
528 characterization of genetic interaction profiles. *Proc Natl Acad Sci U S A* **105**, 5821-6
529 (2008).

530 22. Matsuo, Y. et al. Ubiquitination of stalled ribosome triggers ribosome-associated quality
531 control. *Nat Commun* **8**, 159 (2017).

532 23. Sitron, C.S., Park, J.H. & Brandman, O. Asc1, Hel2, and Slh1 couple translation arrest to
533 nascent chain degradation. *RNA* **23**, 798-810 (2017).

534 24. D'Orazio, K.N. et al. The endonuclease Cue2 cleaves mRNAs at stalled ribosomes during
535 No Go Decay. *Elife* **8**(2019).

536 25. Ikeuchi, K. et al. Collided ribosomes form a unique structural interface to induce Hel2-
537 driven quality control pathways. *EMBO J* **38**(2019).

538 26. Sugiyama, T. et al. Sequential Ubiquitination of Ribosomal Protein uS3 Triggers the
539 Degradation of Non-functional 18S rRNA. *Cell Rep* **26**, 3400-3415 e7 (2019).

540 27. Nishimura, K. & Kanemaki, M.T. Rapid Depletion of Budding Yeast Proteins via the
541 Fusion of an Auxin-Inducible Degron (AID). *Curr Protoc Cell Biol* **64**, 20 9 1-16 (2014).

542 28. Schuller, A.P., Wu, C.C., Dever, T.E., Buskirk, A.R. & Green, R. eIF5A Functions Globally in
543 Translation Elongation and Termination. *Mol Cell* **66**, 194-205 e5 (2017).

544 29. Guydosh, N.R. & Green, R. Dom34 rescues ribosomes in 3' untranslated regions. *Cell*
545 **156**, 950-62 (2014).

546 30. Grollman, A.P. Inhibitors of protein biosynthesis. II. Mode of action of anisomycin. *J Biol*
547 *Chem* **242**, 3226-33 (1967).

548 31. Juszkiewicz, S. & Hegde, R.S. Initiation of Quality Control during Poly(A) Translation
549 Requires Site-Specific Ribosome Ubiquitination. *Mol Cell* **65**, 743-750.e4 (2017).

550 32. Gutierrez, E. et al. eIF5A promotes translation of polyproline motifs. *Mol Cell* **51**, 35-45
551 (2013).

552 33. Pelechano, V. & Alepuz, P. eIF5A facilitates translation termination globally and
553 promotes the elongation of many non polyproline-specific tripeptide sequences. *Nucleic*
554 *Acids Res* **45**, 7326-7338 (2017).

555 34. Doma, M.K. & Parker, R. Endonucleolytic cleavage of eukaryotic mRNAs with stalls in
556 translation elongation. *Nature* **440**, 561-564 (2006).

557 35. Letzring, D.P., Dean, K.M. & Grayhack, E.J. Control of translation efficiency in yeast by
558 codon–anticodon interactions. *RNA* **16**, 2516-2528 (2010).

559 36. Kuroha, K. et al. Receptor for activated C kinase 1 stimulates nascent polypeptide-
560 dependent translation arrest. *EMBO reports* **11**, 956-961 (2010).

561 37. Yan, L.L., Simms, C.L., McLoughlin, F., Vierstra, R.D. & Zaher, H.S. Oxidation and
562 alkylation stresses activate ribosome-quality control. *Nat Commun* **10**, 5611 (2019).

563 38. Vazquez-Laslop, N., Thum, C. & Mankin, A.S. Molecular mechanism of drug-dependent
564 ribosome stalling. *Mol Cell* **30**, 190-202 (2008).

565 39. Dimitrova, L.N., Kuroha, K., Tatematsu, T. & Inada, T. Nascent peptide-dependent
566 translation arrest leads to Not4p-mediated protein degradation by the proteasome. *J*
567 *Biol Chem* **284**, 10343-52 (2009).

568 40. Wilson, D.N. & Beckmann, R. The ribosomal tunnel as a functional environment for
569 nascent polypeptide folding and translational stalling. *Curr Opin Struct Biol* **21**, 274-82
570 (2011).

571 41. Chandrasekaran, V. et al. Mechanism of ribosome stalling during translation of a poly(A)
572 tail. *Nat Struct Mol Biol* **26**, 1132-1140 (2019).

573 42. Davis, A.R., Gohara, D.W. & Yap, M.N. Sequence selectivity of macrolide-induced
574 translational attenuation. *Proc Natl Acad Sci U S A* **111**, 15379-84 (2014).

575 43. Pochopien, A.A. et al. Structure of Gcn1 bound to stalled and colliding 80S ribosomes.
576 *Proc Natl Acad Sci U S A* **118**(2021).

577 44. Wout, P.K., Sattlegger, E., Sullivan, S.M. & Maddock, J.R. Saccharomyces cerevisiae Rbg1
578 protein and its binding partner Gir2 interact on Polyribosomes with Gcn1. *Eukaryot Cell*
579 **8**, 1061-71 (2009).

580 45. Schmidt, C. et al. Structure of the hypusinylated eukaryotic translation factor eIF-5A
581 bound to the ribosome. *Nucleic Acids Res* **44**, 1944-51 (2016).

582 46. Melnikov, S. et al. Crystal Structure of Hypusine-Containing Translation Factor eIF5A
583 Bound to a Rotated Eukaryotic Ribosome. *Journal of molecular biology* **428**, 3570-3576
584 (2016).

585 47. Schmidt, C. et al. The cryo-EM structure of a ribosome–Ski2-Ski3-Ski8 helicase complex.
586 *Science* **354**, 1431-1433 (2016).

587 48. Buschauer, R. et al. The Ccr4-Not complex monitors the translating ribosome for codon
588 optimality. *Science* **368**(2020).

589 49. Lu, L., Lv, Y., Dong, J., Hu, S. & Peng, R. DRG1 is a potential oncogene in lung
590 adenocarcinoma and promotes tumor progression via spindle checkpoint signaling
591 regulation. *Oncotarget* **7**, 72795-72806 (2016).

592 50. Schellhaus, A.K. et al. Developmentally Regulated GTP binding protein 1 (DRG1) controls
593 microtubule dynamics. *Sci Rep* **7**, 9996 (2017).

594 51. Bailey, T.L. et al. MEME SUITE: tools for motif discovery and searching. *Nucleic Acids Res*
595 **37**, W202-8 (2009).

596

METHODS

Yeast strains, plasmid constructs and growth conditions

Saccharomyces cerevisiae strains with BY4742 (*MATα his3Δ1 leu2Δ0 lys2Δ0 ura3Δ0*) background were used in this study. Chromosomal insertion and knockout strains with this background were obtained by established homologous recombination techniques [1,2], and are listed in **Supplemental Table 1**. The plasmids used here were constructed via standard cloning strategies and are listed in **Supplemental Table 2**. To generate C-terminal, chromosomally TAP-tagged strains, the TAP-*URA3* cassette, contained in the modified p415G plasmid, was amplified with homology regions to replace the stop codon of the gene to be tagged. Strains were confirmed by sequencing across the entire fusion gene, as well as western blot detection of the calmodulin binding peptide (CBP) epitope. It has been reported that cellular growth of the Δ*rbg1*Δ*rbg2*Δ*slh1*Δ strain was severely impaired [3]. To control the Rbg1 protein level in the cell, a mini auxin-inducible degron (mAID) tag was inserted chromosomally into the Δ*rbg2*Δ*slh1* strain, at the 5' end of the Rbg1 gene, with a sequence containing the *KanMX*-GAL10p-mAID-Flag epitope before the start codon of Rbg1 [4].

Genes encoding Rbg1 and Tma46 were amplified from the genomic DNA of *S. cerevisiae* and were cloned into modified pET28a or pET22b vectors using standard cloning strategies. Mutants were generated by mutagenesis PCR using the Q5 Site-Directed Mutagenesis Kit (NEB), according to the manufacturer's instructions.

22 To obtain polysome profiles and perform 5Pseq experiments, wild type and mutant cells
23 were grown to an OD_{600} of 0.6 in YPGR (2% galactose + 0.2% raffinose) medium at 30 ˚C,
24 harvested by centrifugation, then washed and resuspended in the same volume of YEPD (2%
25 glucose) medium containing 1 mM auxin (Sigma). These cells were grown in the presence of
26 auxin for another 20 minutes at 30 ˚C to deplete Rbg1 completely.

27

28

29 **Purification of ribosomes, proteins**

30 Yeast ribosomes from the YAS2488 strain were purified according to published
31 methods[5]. Wild type and mutant Rbg1 and Tma46 were cloned and co-overexpressed in
32 BL21(DE3) cells, then purified by affinity and ion-exchange chromatography [6].

33

34

35 **Ribosome binding assay**

36 Purified Rbg1/Tma46 or Rbg1/Tam46-ΔZnF complexes were incubated with GDPCP or
37 GDP for 15 minutes at 30 ˚C in polysome lysis buffer (20 mM Tris-HCl, pH 8.0, 140 mM KCl,
38 1.5 mM $MgCl_2$, 1% (v/v) Triton X-100, 1 mM DTT, 100 µg/ml cycloheximide) followed by
39 addition of purified 80S for another 30 minutes. The factor-bound ribosomal complexes were
40 then separated by sedimentation through a 10-50% sucrose gradient in polysome lysis buffer.
41 Binding of Rbg1/Tma46 to the ribosome was determined by western blot. Flag-tagged RPL25
42 was immunoblotted as control.

43

44

45 **Cell growth assay**

46 Cell growth rates were determined by a spot assay as reported [7] with minor
47 modifications. Cells were first grown to exponential phase at 30 ˚C in either YPGR or YEPD,
48 depending upon the strain used. Then 0.5 OD_{600} units of cells were pelleted down and
49 resuspended in 0.5 ml of 1X PBS buffer. The following serial dilutions were prepared in 1 x PBS
50 buffer: 1/5, 1/25, 1/125, and 1/625, and 1 µl of each dilution was spotted on YEPD agar plates. 1
51 mM auxin (Sigma) was added for assays of Δrbg2Δslh1-Rbg1d strains. Images were taken after
52 2 to 5 days of growth at 30 ˚C.

53

54

55 **Polysome profiling**

56 Yeast cells were grown at 30 ˚C until they reached an OD_{600} of 0.6, then were treated
57 with 100 µg/ml of cycloheximide for 2 minutes before harvesting. Cells were quickly harvested
58 by centrifugation and were washed twice with ice-cold polysome lysis buffer. The cell pellet was
59 resuspended in 1 ml of polysome lysis buffer supplemented with EDTA-free protease inhibitors
60 (Roche) and was grounded in liquid nitrogen using an RNase-free mortar and pestle. Extracts
61 were clarified at 18,000 × *g* for 10 minutes at 4 ˚C, then loaded onto 10%-50% sucrose gradients
62 in polysome gradient buffer (20 mM Tris-HCl, pH 8.0, 140 mM KCl, 5 mM $MgCl_2$, 20 U/ml
63 SUPERase.In, 0.5 mM DTT, 100 µg/ml cycloheximide). Gradients were centrifuged at 32,000
64 rpm for 3 hours and 45 minutes in a Beckman SW 32.1 Ti rotor and polysome profiles were
65 generated by fractionation with continuous measurement of absorbance at 260 nm.

66

67

68 **Western blot**

69 Western blotting was performed as described [8]. Fractions from polysome profiles were
70 resolved via SDS-PAGE, and proteins of interest were transferred to nitrocellulose membranes
71 (GE Healthcare Amersham) for 40 minutes at 100 V in a Mini Trans-Blot apparatus (Bio-Rad).
72 Protein bands were detected with either anti-Flag (Sigma-Aldrich) or anti-His antibodies (Sigma-
73 Aldrich).

74

75

76 **5Pseq library preparation**

77 5Pseq libraries were prepared as described [9,10]. Yeast strains were grown in 50 ml YPGR
78 medium until they reached an OD_{600} of 0.6. Cells were then harvested, and their media
79 exchanged for 50 ml YEPD containing 1 mM auxin (Sigma), followed by an additional 20
80 minutes of incubation. Cells were harvested quickly by centrifugation. Total RNA was extracted,
81 and DNA was removed by incubation with TURBO DNase (Ambion) for 30 minutes at 37 ˚C.
82 For control libraries, 50 µg of DNA-free total RNA was fragmented by incubation at 80 ˚C for 5
83 minutes in RNA fragmentation buffer (40 mM Tris-acetate, pH 8.1, 100 mM KOAc, 30 mM
84 $Mg(OAc)_2$). Fragmented 5'-OH sites were phosphorylated by treatment with 5 units of T4
85 polynucleotide kinase (NEB) for 1 hour at 37 ˚C, followed by phenol:chloroform extraction. The
86 phosphorylated 5'-ends were subjected to RNA ligation by 20 units of T4 RNA ligase 1 (NEB)
87 in the presence of 10 mM DNA/RNA rP5_RND oligo (**Supplemental Table 3**) at 16 ˚C

88 overnight. For the 5Pseq libraries, 50 µg of DNA-free total RNA was directly ligated to the
89 rP5_RND oligo in the same conditions as specified for control samples. The polyadenylated
90 mRNAs were enriched using Dynabeads $(dT)_{25}$ (Life Technologies), according to the
91 manufacturer's instructions, followed by fragmentation for 5 minutes at 80˚C in RNA
92 fragmentation buffer. Both the controls and 5' RNA-seq samples were primed with random
93 hexamers and reverse transcribed with Superscript II (Life Technologies). Second strand cDNA
94 synthesis was performed using a single PCR cycle (98 ˚C for 1 minute, 50 ˚C for 2 minutes, and
95 72 ˚C for 15 minutes) in Phusion High-Fidelity PCR Master Mix and was primed with BioNotI-
96 P5-PET (**Supplemental Table 3**). Double-stranded cDNA was purified using HighPrep beads
97 (Magbio), then was bound to Dynabeads M-280 Streptavidin beads (Life Technologies). Bound
98 DNA molecules were subjected to end repair, adenine addition, and adaptor ligation via addition
99 of 0.5 µL of P7MPX annealed adaptor, which was prepared by annealing the P7MPX_linker_for
100 and P7MPX_linker_rev (**Supplemental Table 3**) primers at a final concentration of 2.5 µM. The
101 Dynabead-bound DNA was washed and subjected to PCR amplification (98 ˚C for 30 seconds;
102 18 cycles of the following condition: 98 ˚C for 20 seconds, 65 ˚C for 30 seconds, 72 ˚C for 30
103 seconds; 72 ˚C for 5 minutes) using Phusion High-Fidelity PCR Master Mix with HF buffer
104 (NEB), 0.1 µM of PE1.0, and the appropriate PE2_MPX_01 to PE2_MPX_08 primers
105 (**Supplemental Table 3**). Samples were size-selected using 0.6x-0.9x (v/v) HighPrep beads
106 (Magbio), separated via agarose gel electrophoresis, and the 300-500 bp regions of the gel were
107 extracted. Libraries were sequenced using single-end, 100bp-read NovaSeq Illumina sequencing
108 with 6 nt indexing reads for library identification.

109

110

111 **High throughput sequencing data processing and analysis**

112 For all libraries, reads were first demultiplexed using the index sequences. The 3' adaptor
113 sequence was identified and removed using the cutadapt package [11]. After adaptor removal, the
114 remaining reads were deduplicated by bbmap (BBMap - Bushnell B. -
115 sourceforge.net/projects/bbmap/) based upon random barcode sequences, and the 5' UMI were
116 trimmed by fastx_trimmer (Hannon, G.J. (2010) FASTX-Toolkit.). Non-coding RNAs were
117 filtered by mapping to annotated *S. cerevisiae* rRNAs, tRNAs, snRNAs, and snoRNAs using
118 Bowtie1 [12]. Unaligned reads were then mapped to the sacCer3 genome using Bowtie2 [13] with the
119 arguments: '--local -D 15 -R 2 -N 1 -L 20 -i S,1,0.75 -S'.

120

121 Unless indicated otherwise, data analysis was performed using a series of custom scripts
122 written in Python. For 5Pseq experiment, reads with multiple alignments, mapping quality values
123 < 30, or those containing soft-clipped bases on the 5' end were excluded from downstream
124 analysis. The 5' ends of reads passing quality filtering were extracted and the total numbers of
125 reads per genome location were calculated. Reads per million (RPM) values for each genomic
126 locus were calculated using the number of unique reads. Only genes with reads per million per
127 kilobase (RPKM) values of greater than 20 were chosen for further analysis. To create meta gene
128 plots, we calculated the average rpm of the 5' ends from all biological replicates. These 5' ends
129 were then aligned relative to the stop codon (or any specific codon) of all ORFs, and the sum of
130 the 5' ends reads was determined at each position. To analyze ribosome pausing around the start
131 codon, genes were sorted by a ratio value which is calculated by dividing the read counts at -14
132 nt or 4 nt by the total read counts corresponding to the surrounding ±2 codons, as previously
133 described [10]. Then the first 8 amino acids of the ORF were extracted. Sequences of the top 50%

134 of genes were compared to the bottom 50% using MEME [14]. To characterize the elongation
135 pausing, we calculated the pause score, as described previously, with minor modifications [15].
136 Pause scores were calculated by dividing the rpm value at each genomic position by the mean of
137 the rpm values in the ±10-codon region surrounding the position. Regions in the first and last 10
138 codons of the ORF were excluded. Amino acid sequences with pause scores > 10 were
139 considered to be stalling sites. Stalling sequences were calculated by MEME [14] using the
140 sequences with pause score <10 as a control.

141

142

143 **Flow cytometry**

144 Overnight cultured cells carrying the dual fluorescence reporter gene with a stalling
145 sequence containing twelve consecutive arginine codons were first inoculated into 50 ml YEPD
146 with initial OD_{600} = 0.1 and grown to mid-log phase at 30 ˚C. Cells were then collected and
147 diluted to OD_{600}=0.1 and about 10,000 cells were analyzed with a FACSCanto SORP flow
148 cytometer (Made, company) for GFP and mCherry fluorescence detection using 488 nm and 561
149 nm excitation lasers, respectively. Scatter plots show the intensity of GFP and mCherry for
150 individual cells. Flow cytometry was done in triplicate.

151

152

153 **Electron microscopy, data collection and image processing**

154 Saccharomyces cerevisiae with C-terminally TAP-tagged Rbg1 were grown to log phase
155 at 30 ˚C, then were treated with 100 µg/ml of cycloheximide for 2 minutes before being

156 harvested by centrifugation. The harvested cells were resuspended in one-third of polysome lysis
157 buffer and were grounded in liquid nitrogen. Cell extracts were clarified at 20,000 × *g* for 30
158 minutes at 4 ˚C and incubated with IgG beads for 1 hour at 4˚C. The complex-bound beads were
159 washed three times with polysome lysis buffer, and the Rbg1/Tma46 bound ribosomal
160 complexes were eluted by incubating with TEV for 1 hour at 20 ˚C. 0.05% glutaraldehyde was
161 added to the eluted complex and incubated for 30 minutes on ice. The crosslinking reaction was
162 quenched by 25 mM Tris-HCl (pH 7.5) and 0.01% n-dodecyl-D-maltoside (DDM) was added to
163 the final solution. Sample preparation for cryoEM studies was performed as described [16]. 2.5 µl
164 aliquots of ribosomal complexes were incubated for 30 seconds on glow-discharged Holley
165 carbon grids with a thin-layer carbon film cover (Quantifoil). Grids were blotted using a Vitrobot
166 Mark IV (FEI) for 3 seconds in 100% humidity at 4 ˚C, then were plunge frozen into liquid
167 ethane. Data were collected in vitreous ice using Titan Krios G3i (D3796) transmission electron
168 microscopes operating at 300 keV with FEI Falcon III detectors. A total of 11,529 micrographs
169 were acquired using a dose of 30 $e^{-}Å^{-2}$. The drifts of movie frames were corrected using
170 MotionCor2 [17], and the contrast transfer functions were determined using CTFFIND4 [18]. Data
171 processing was carried out in Relion3 [19]. A total of 1,222,865 particles were picked and extracted
172 for reference-free 2D classification. 737,448 particles were selected and subjected to 3D
173 refinement program followed by 3D classification with a mask around the ribosome GTPase
174 association center. The class displaying good factor density (95,380 particles) were subjected to
175 3D refinement to yield a reconstruction at 3.23 Å. Resolutions were reported based upon the
176 gold-standard Fourier shell correlation (FSC) of 0.143 criterion [20].

177

178

179 **Model building, refinement and validation**

180 The high-resolution crystal structure of the yeast 80S (PDB: 4V88) [21] was used and fit
181 into the EM density map using rigid body fitting in Chimera[22]. The body, head and shoulder
182 domains of 40S, L1 stalk and P stalk of 60S were fit separately using Coot [23]. Ribosome-bound
183 ligands, A-tRNA, P-tRNA and eIF5A, were built into density map in Coot using PDB 5GAK as
184 a reference [24]. The crystal structure of Rbg1/Tma46 complex (PDB: 4A9A) [6] was used a
185 reference, and the HTH, S5D2L, G domain, TGS domain of Rbg1 and each helix of Tma46 were
186 built into the density map accordingly. The second zinc finger of Tma46 was built using the
187 homology model generated by SWISS-MODEL [25].

188 The model obtained was refined using Phenix with secondary structure, RNA base-pair,
189 sugar pucker and base stacking restraints. The final model was validated using MolProbity [26].
190 Refinement statistics for the structures were summarized in **Supplemental Table 4**. Figures
191 were made in Chimera [22] and Pymol [27].

192

193

194 **Data availability**

195 The sequencing data for 5P-seq experiment have been deposited in NCBI's Gene
196 Expression Omnibus and are accessible through GEO series accession numbers GSE154212.
197 Electron microscopy maps have been deposited in the Electron Microscopy Data Bank under
198 accession codes EMD-xxxx. Coordinates have been deposited in the Protein Data Bank under
199 accession code xxxx.

200

Acknowledgments

We thank Prof. Peter Moore at Yale University for critical comments of the manuscript. We also thank the Cryo-EM Center at Southern University of Science and Technology, Junyi Jiang and Qingrong Li in the F. Zeng laboratory, Dr. Bridget Carragher and Dr. Ed Eng at the National Center for CryoEM Access and Training (NCCAT) and Dr. Valerie Tokars at Northwestern University for their help on cryoEM data collection, the core Research Facility at Southern University of Science and Technology for flow cytometry, Roy J. Carver Biotechnology Center at the University of Illinois at Urbana-Champaign for sequencing and members in the H. Jin laboratory for helpful discussions. H.J. acknowledges support from the National Institute of General Medical Sciences of the NIH (R01-GM120552).

All authors declare no conflict of interests

REFERENCES

1. Baudin, A., Ozier-Kalogeropoulos, O., Denouel, A., Lacroute, F. & Cullin, C. A simple and efficient method for direct gene deletion in Saccharomyces cerevisiae. *Nucleic Acids Res* **21**, 3329-30 (1993).

222 2. Longtine, M.S. et al. Additional modules for versatile and economical PCR-based gene
223 deletion and modification in Saccharomyces cerevisiae. *Yeast* **14**, 953-61 (1998).
224 3. Daugeron, M.C., Prouteau, M., Lacroute, F. & Seraphin, B. The highly conserved
225 eukaryotic DRG factors are required for efficient translation in a manner redundant with
226 the putative RNA helicase Slh1. *Nucleic Acids Res* **39**, 2221-33 (2011).
227 4. Schuller, A.P., Wu, C.C., Dever, T.E., Buskirk, A.R. & Green, R. eIF5A Functions Globally in
228 Translation Elongation and Termination. *Mol Cell* **66**, 194-205 e5 (2017).
229 5. Acker, M.G., Kolitz, S.E., Mitchell, S.F., Nanda, J.S. & Lorsch, J.R. Reconstitution of yeast
230 translation initiation. *Methods Enzymol* **430**, 111-45 (2007).
231 6. Francis, S.M., Gas, M.E., Daugeron, M.C., Bravo, J. & Seraphin, B. Rbg1-Tma46 dimer
232 structure reveals new functional domains and their role in polysome recruitment.
233 *Nucleic Acids Res* **40**, 11100-14 (2012).
234 7. Xu, X., Lambrecht, A.D. & Xiao, W. Yeast survival and growth assays. *Methods Mol Biol*
235 **1163**, 183-91 (2014).
236 8. Zeng, F. & Jin, H. Peptide release promoted by methylated RF2 and ArfA in nonstop
237 translation is achieved by an induced-fit mechanism. *RNA* **22**, 49-60 (2016).
238 9. Pelechano, V., Wei, W. & Steinmetz, L.M. Genome-wide quantification of 5'-
239 phosphorylated mRNA degradation intermediates for analysis of ribosome dynamics.
240 *Nat Protoc* **11**, 359-76 (2016).
241 10. Pelechano, V., Wei, W. & Steinmetz, L.M. Widespread Co-translational RNA Decay
242 Reveals Ribosome Dynamics. *Cell* **161**, 1400-12 (2015).

243 11. Martin, M. Cutadapt removes adapter sequences from high-throughput sequencing
244 reads. *2011* **17**, 3 (2011).
245 12. Langmead, B., Trapnell, C., Pop, M. & Salzberg, S.L. Ultrafast and memory-efficient
246 alignment of short DNA sequences to the human genome. *Genome Biol* **10**, R25 (2009).
247 13. Langmead, B. & Salzberg, S.L. Fast gapped-read alignment with Bowtie 2. *Nat Methods*
248 **9**, 357-9 (2012).
249 14. Bailey, T.L. et al. MEME SUITE: tools for motif discovery and searching. *Nucleic Acids Res*
250 **37**, W202-8 (2009).
251 15. Guydosh, N.R. & Green, R. Dom34 rescues ribosomes in 3' untranslated regions. *Cell*
252 **156**, 950-62 (2014).
253 16. Zeng, F. et al. Structural basis of co-translational quality control by ArfA and RF2 bound
254 to ribosome. *Nature* **541**, 554-557 (2017).
255 17. Zheng, S.Q. et al. MotionCor2: anisotropic correction of beam-induced motion for
256 improved cryo-electron microscopy. *Nat Methods* **14**, 331-332 (2017).
257 18. Rohou, A. & Grigorieff, N. CTFFIND4: Fast and accurate defocus estimation from
258 electron micrographs. *J Struct Biol* **192**, 216-21 (2015).
259 19. Zivanov, J. et al. New tools for automated high-resolution cryo-EM structure
260 determination in RELION-3. *Elife* **7**(2018).
261 20. Scheres, S.H. & Chen, S. Prevention of overfitting in cryo-EM structure determination.
262 *Nat Methods* **9**, 853-4 (2012).
263 21. Ben-Shem, A. et al. The Structure of the Eukaryotic Ribosome at 3.0 Å Resolution.
264 *Science* **334**, 1524-1529 (2011).

265 22. Pettersen, E.F. et al. UCSF Chimera--a visualization system for exploratory research and
266 analysis. *J Comput Chem* **25**, 1605-12 (2004).
267 23. Emsley, P., Lohkamp, B., Scott, W.G. & Cowtan, K. Features and development of Coot.
268 *Acta Crystallographica Section D* **66**, 486-501 (2010).
269 24. Schmidt, C. et al. Structure of the hypusinylated eukaryotic translation factor eIF-5A
270 bound to the ribosome. *Nucleic Acids Res* **44**, 1944-51 (2016).
271 25. Waterhouse, A. et al. SWISS-MODEL: homology modelling of protein structures and
272 complexes. *Nucleic Acids Research* **46**, W296-W303 (2018).
273 26. Williams, C.J. et al. MolProbity: More and better reference data for improved all-atom
274 structure validation. *Protein Science* **27**, 293-315 (2018).
275 27. Schrodinger, LLC. The PyMOL Molecular Graphics System, Version 1.8. (2015).
276

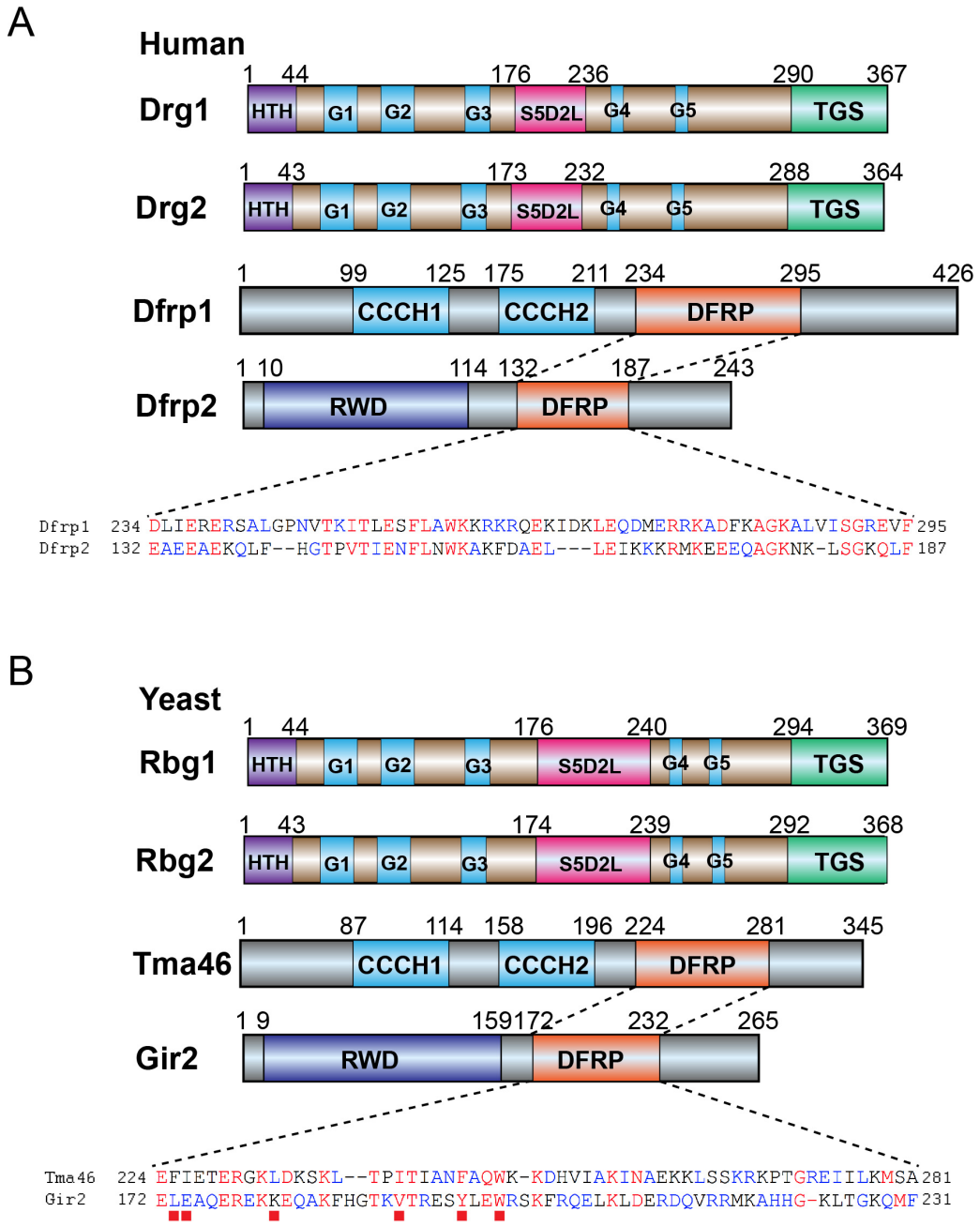

Supplemental Figure 1. Overview of the domain organization of the Drg/Dfrp proteins in humans and yeast. Sequence alignments are shown for the DFRP domains. Red squares (■) indicate hydrophobic residues in Tma46 that interact with Rbg1 when the heterodimeric complex Rbg1/Tma46 binds to the ribosome seen from the structure obtained in this study.

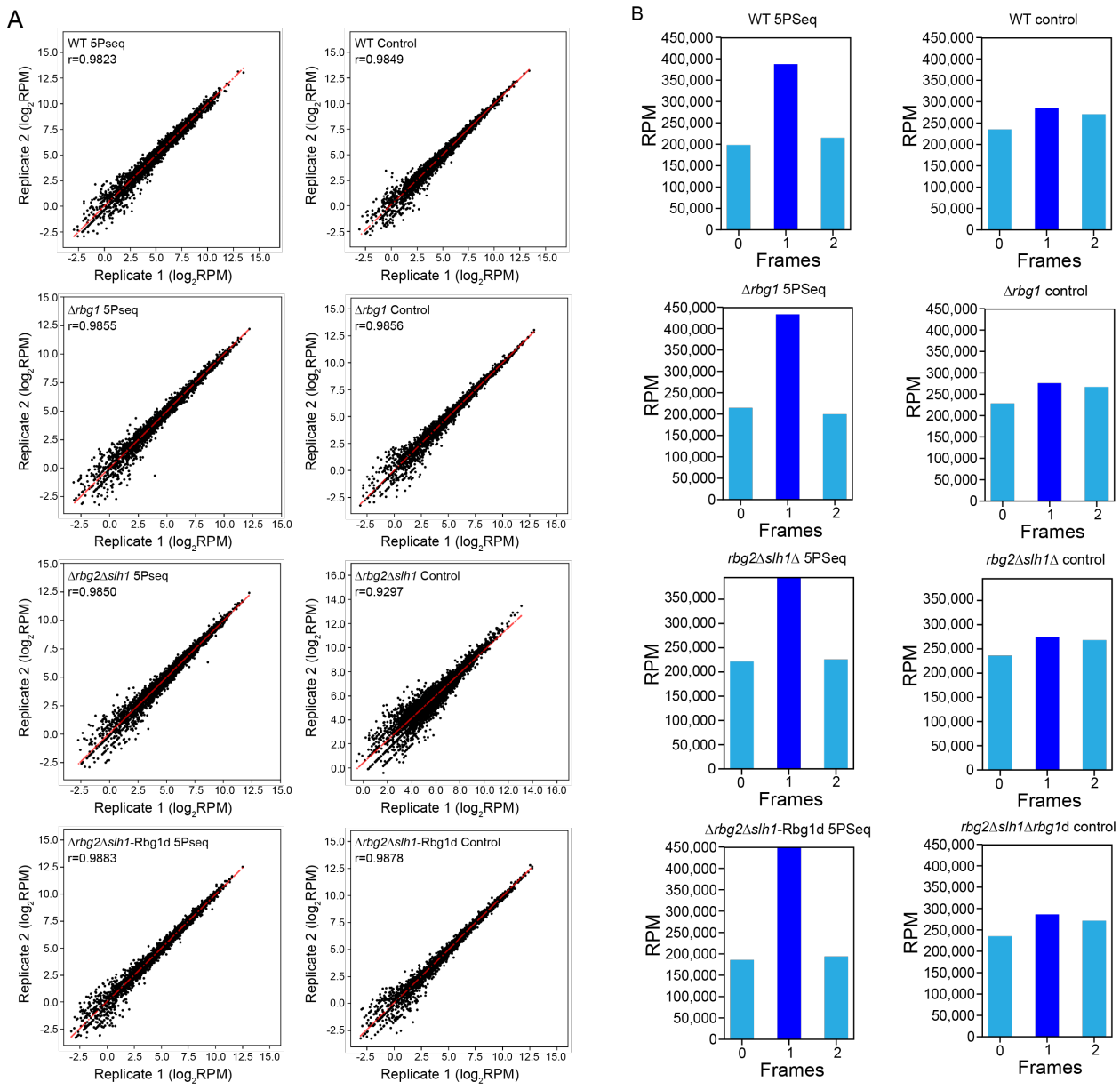

Supplemental Figure 2. Data quality of 5PSeq experiments performed with different strains

A Scatter plots showing reproducibility of 5Pseq data between biological replicates for 5Pseq (Left) and controls (Right). Reads with multiple alignments, mapping quality < 30, or those containing soft-clipped bases on the 5' end were excluded. Reads were normalized to the library

size using RPM (reads per million). Results for the two biological replicates are compared, and Pearson correlation coefficients for each comparison are shown.

B 3-nt periodicity pattern of the 5P-seq data. The 5' ends of reads were extracted and the total number of reads at each frame were calculated and are displayed as histograms for all of the codons along the coding region of all genes. Because the ribosome protected region in 5P-seq is 14 nt from the 5' end to the P-site of the ribosome, the 5Pseq shows a peak at frame 1. Control samples were also analyzed in the same manner and show no preferred peak among the three frames.

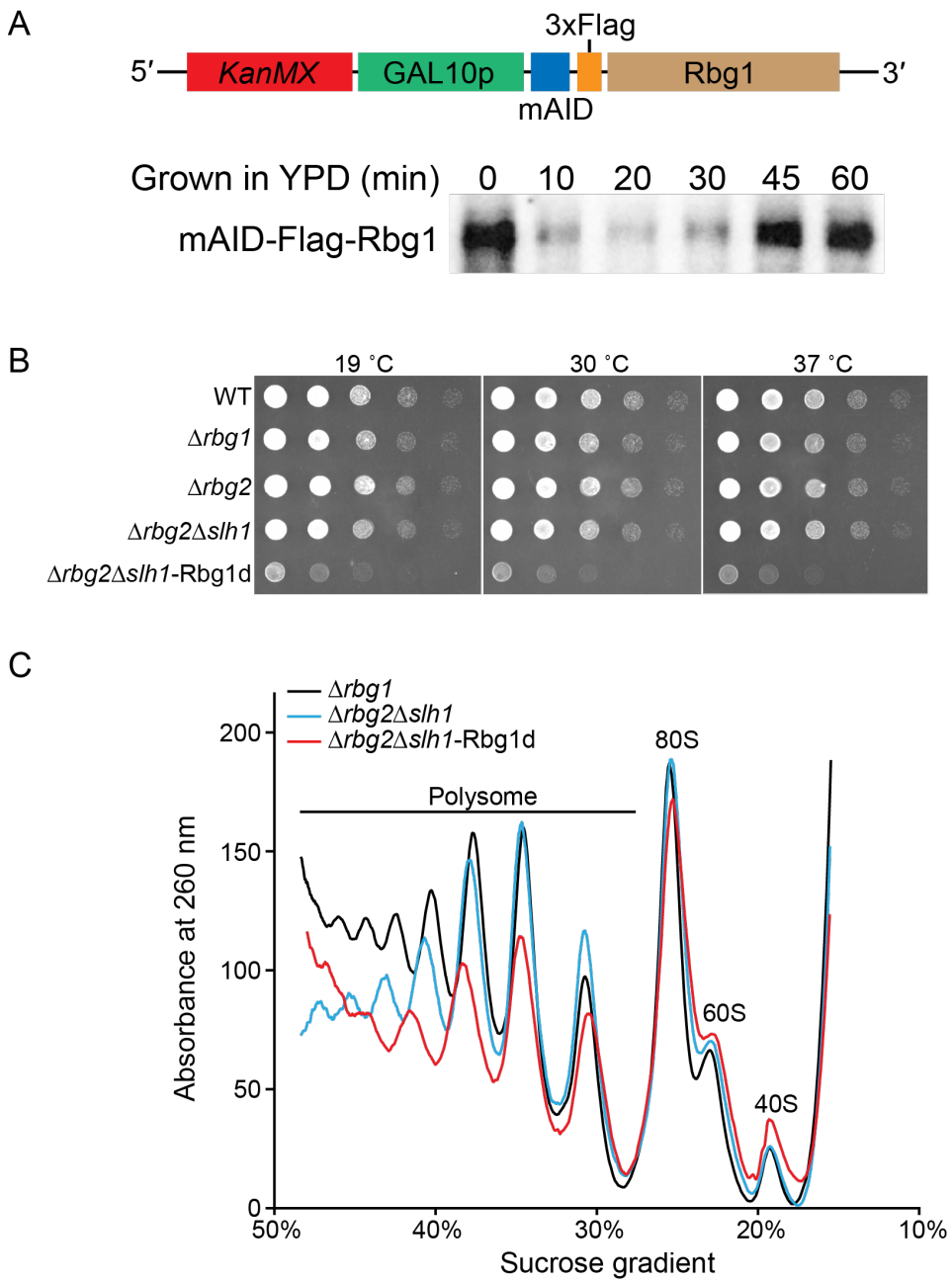

23

24

25 **Supplemental Figure 3. Rbg proteins play important roles in global translation.**

26 **A.** Model of the auxin inducible-degron system. To remove the Rbg1 protein from the cell, a

27 GAL10 promoter was inserted into the 5'UTR of rbg1 gene so that the Rbg1 transcription levels

28 can be controlled by the presence of glucose in the media. A mini auxin-inducible degron

29 (mAID) tag was fused to the N-terminus of Rbg1. Cells were first grown in YPGR medium and
30 then changed to YEPD medium containing 1 mM auxin to induce the degradation of Rbg1
31 protein in the cell. Aliquots at different time points were acquired and the Rbg1 protein levels
32 were monitored by western blot with anti-Flag antibody. With the mAID degron tag, Rbg1
33 protein degrades after 20 minutes but its expression is restored after 45 minutes.

34 **B.** Elimination of Rbg1 under Δrbg2Δslh1 background shows a temperature-independent growth
35 defect. Serial dilutions of liquid cultures growing in exponential phase were spotted on YEPD
36 plates containing 1 mM auxin and were incubated for 2 days at 30 ˚C or 37 ˚C, or for 4 days at
37 19 ˚C.

38 **C.** Polysome profiles from cells incubated for 20 minutes in YEPD indicate that Rbg1 plays an
39 important role in global translation. Cells were first grown in YPGR medium to OD_{600} 0.6, then
40 were changed to YEPD medium containing 1 mM auxin for 20 minutes. Cells were then quickly
41 harvested and polysome profiling was performed. The profiles of WT and Δrbg2 strains are not
42 shown here since WT, Δrbg2, and Δrbg1 have nearly identical profiles. These data represent one
43 of three biological replicates.

44

45

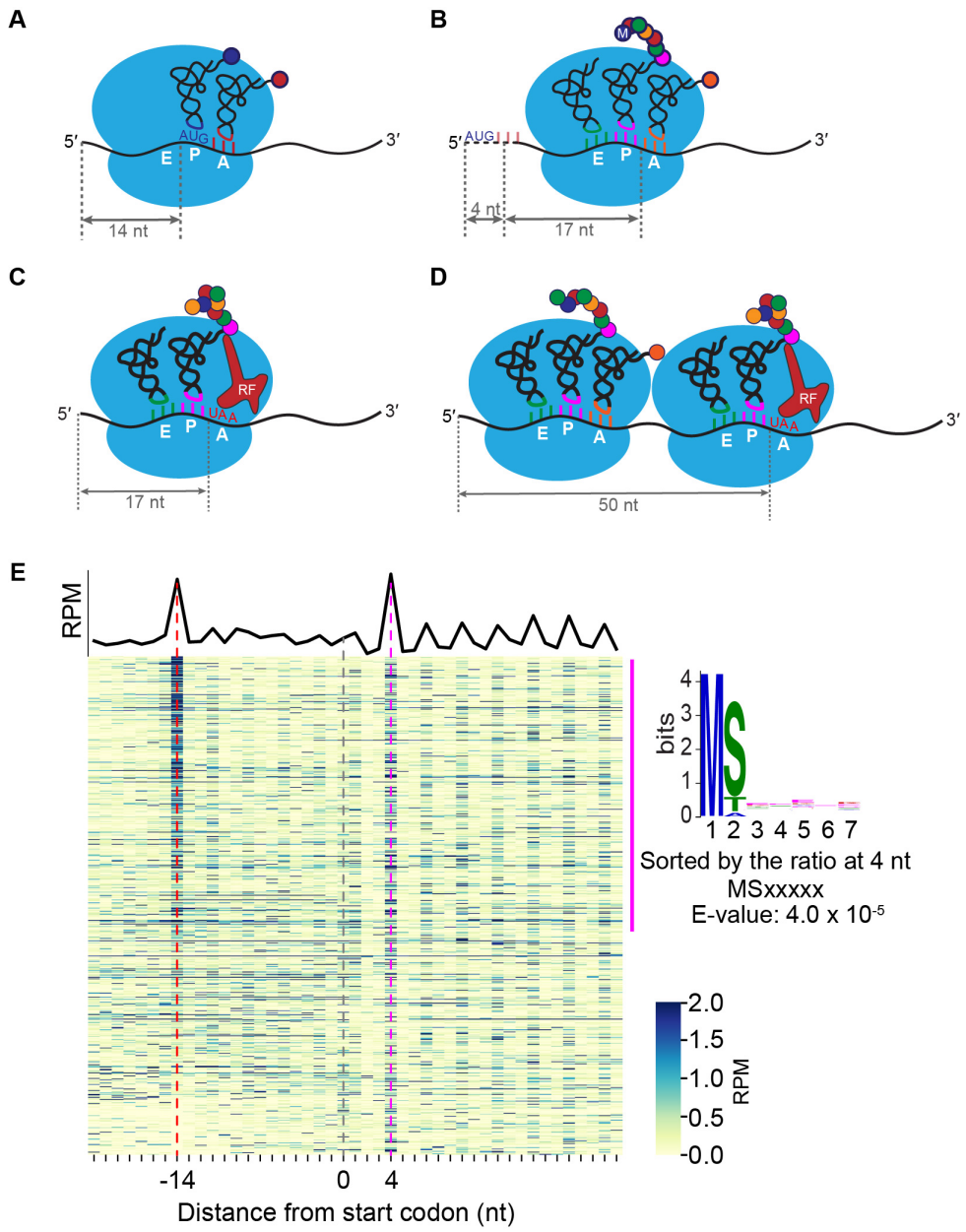

Supplemental Figure 4. Ribosome pausing at the initiation and termination sites are sequence independent.

A to **D**. Models for mRNA footprints generated by 5Pseq for stalling peaks at -14 nt (**A**) and 4 nt (**B**) at the initiation codon, and -17 nt (**C**) and -50 nt (**D**) at the termination codon. The length between the 5' end and P-site in the traditional ribosome profiling method is 12-13 nt. Due to

52 the steric hindrance between the ribosome and exonuclease Xrn1, the length between the 5' end
53 of the mRNA and the P-site is 14 nt for 5Pseq.

54 **E**. A metagene representing both the average coverage (black line), and gene-specific coverage
55 (blue heatmap) for the Δrbg2Δslh1-Rbg1d mutant. Only genes with RPM values larger than five
56 in the displayed regions were considered. Genes were sorted by the ratio of reads at either the -14
57 nt (red dotted line) or 4 nt (magenta dotted line) positions to the reads corresponding to the
58 surrounding ± 2 codons. To identify specific peptide sequences, the first eight amino acids of the
59 genes in the top 50% were compared to the bottom half using MEME [1]. No sequence motif was
60 found by MEME for the genes sorted at -14 nt, and the sequence motif MSxxxxx was found for
61 the genes sorted at 4nt position. .

62

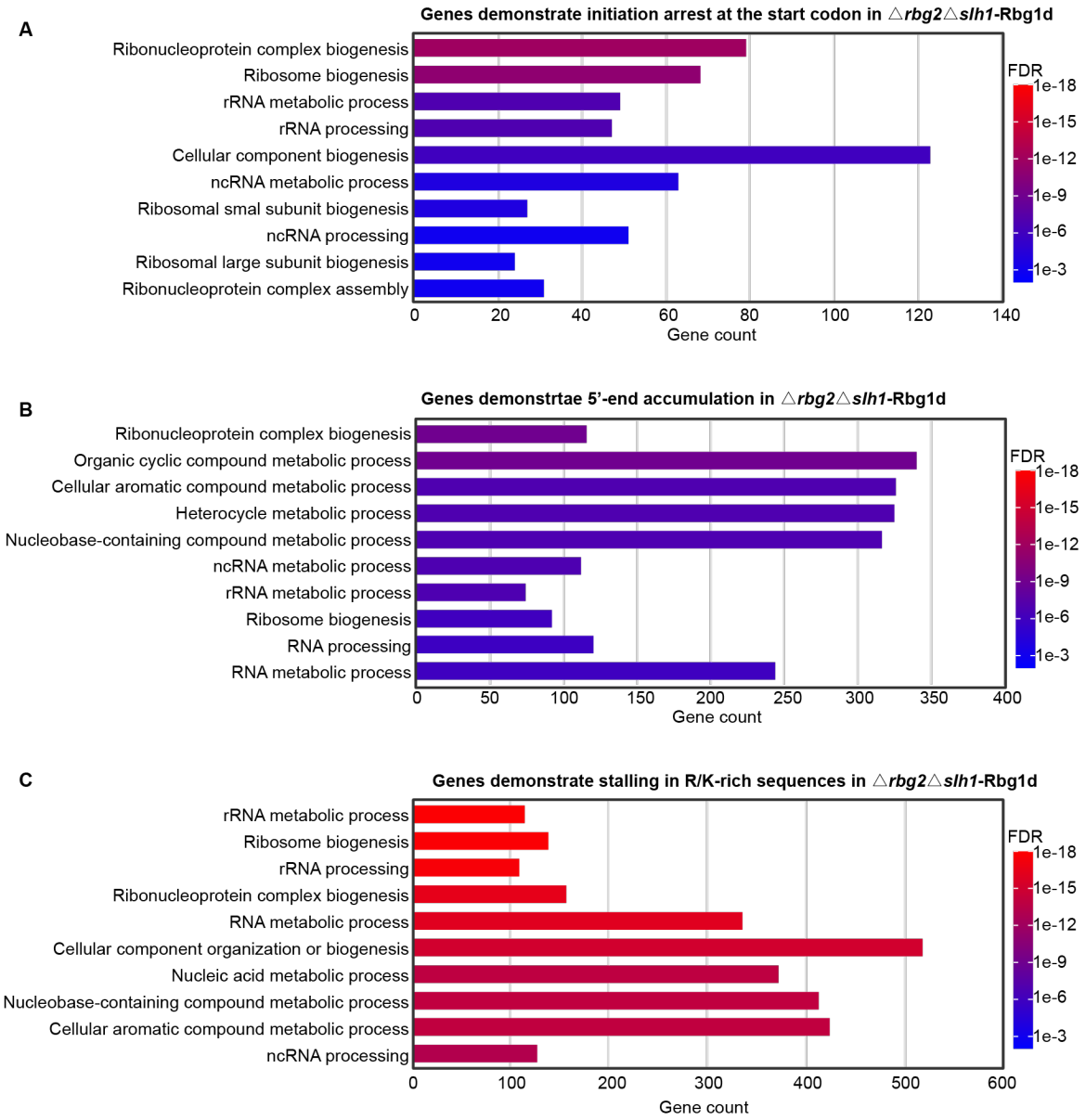

63

64 **Supplemental Figure 5. Gene ontology analysis for genes demonstrate initiation arrest, 5'-**

65 **end accumulation and elongation stalling in R/K-rich sequences**

66 **A**. Gene ontology analysis of genes showing ribosome pausing at the initiation site in the

67 Δrbg2Δslh1-Rbg1d cell. By filtering the ratio of reads at -14 nt to the surrounding ± 2 codons

68 larger than 0.1, 353 genes were selected from the Δrbg2Δslh1-Rbg1d strain for Gene ontology

69 analysis using DAVID [2]. The top 10 gene ontology terms for biological processes were shown,
70 ranked by false discovery rate (FDR).

71 **B**. Gene ontology analysis of the 715 genes which have higher proportion scores in the
72 Δrbg2Δslh1-Rbg1d cell comparing to WT cell. The range of -12 nt to 99 nt, with respect to the
73 first base of start codon, was used to calculate the proportion score. Genes whose proportion
74 scores were larger than 0.4 in the Δrbg2Δslh1-Rbg1d cell, and whose proportion scores were
75 more than 1.5 times the scores found in the WT cell were selected and analyzed by DAVID [2].
76 The top 10 GO terms for biological processes are shown, ranked by false discovery rate (FDR).

77 **C.** Gene ontology analysis of the 993 genes that have pause score larger than 10 in Δrbg2Δslh1-
78 Rbg1d cell. The top 10 gene ontology terms for biological process were shown, ranked by false
79 discovery rate (FDR).

80

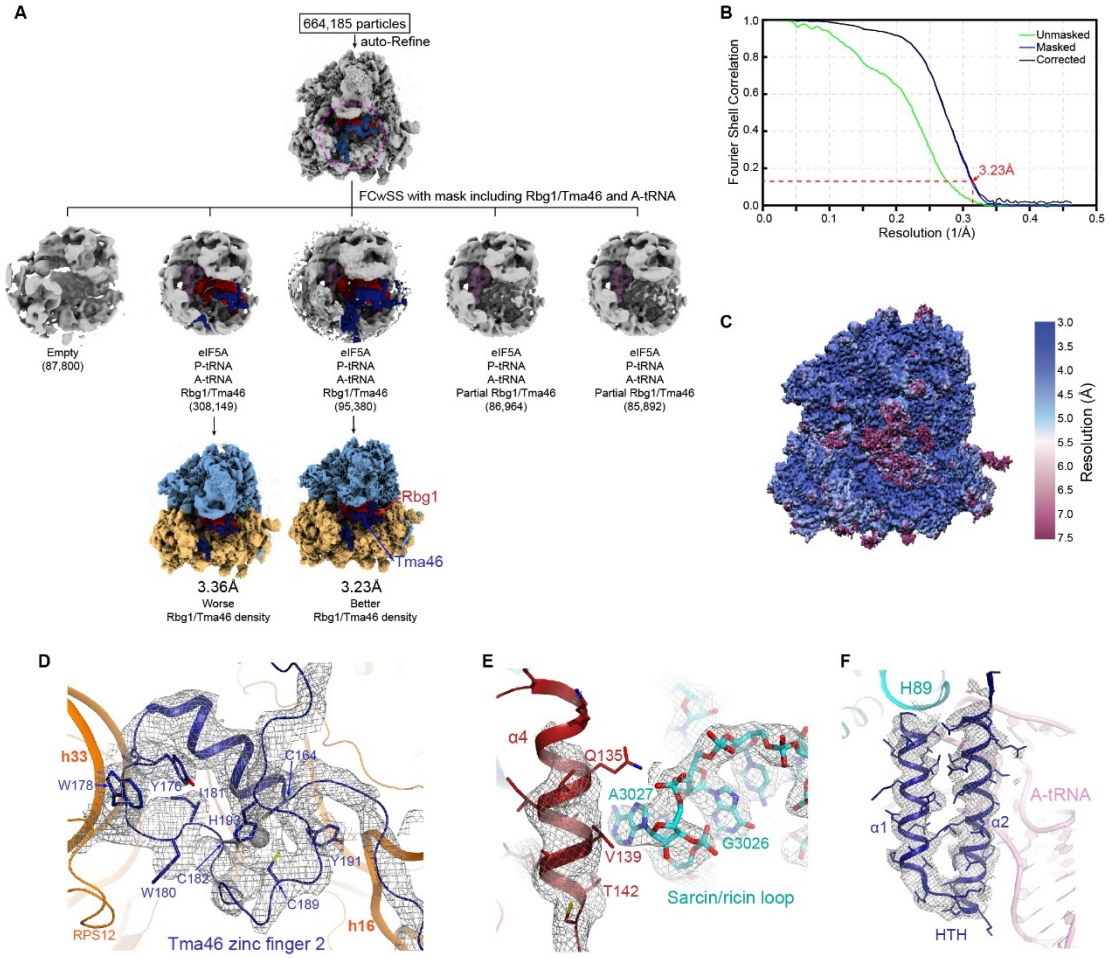

Supplemental Figure 6. Structure determination of Rbg1/Tma46 on the ribosome and map quality.

A. Focused classification with subtracted signal (FCwSS) with the mask over the Rbg1/Tma46 was performed on the selected 664,185 particles from 2D classification. Two of the five classes bound with Rbg1/Tma46 yielded 3.36 Å and 3.23 Å resolution, respectively. The two reconstructions are the same regarding to the conformation of proteins or ribosome. Only the 3.23 Å reconstruction which has better Rbg1/Tma46 density was used in this study.

91 **B**. Gold-standard Fourier shell correlation (FSC) curves for the reported cryoEM reconstruction.

92 **C**. The density map coloured by local resolution in surface view for the entire ribosomal

93 complex.

94 **D-F**. Representative electron microscopy maps showing the refined structures of zinc finger of

95 Tma46 (**D**), sarcin/ricin loop of the large ribosomal subunit (**E**) and HTH domain of Rbg1 (**F**).

96

97

98

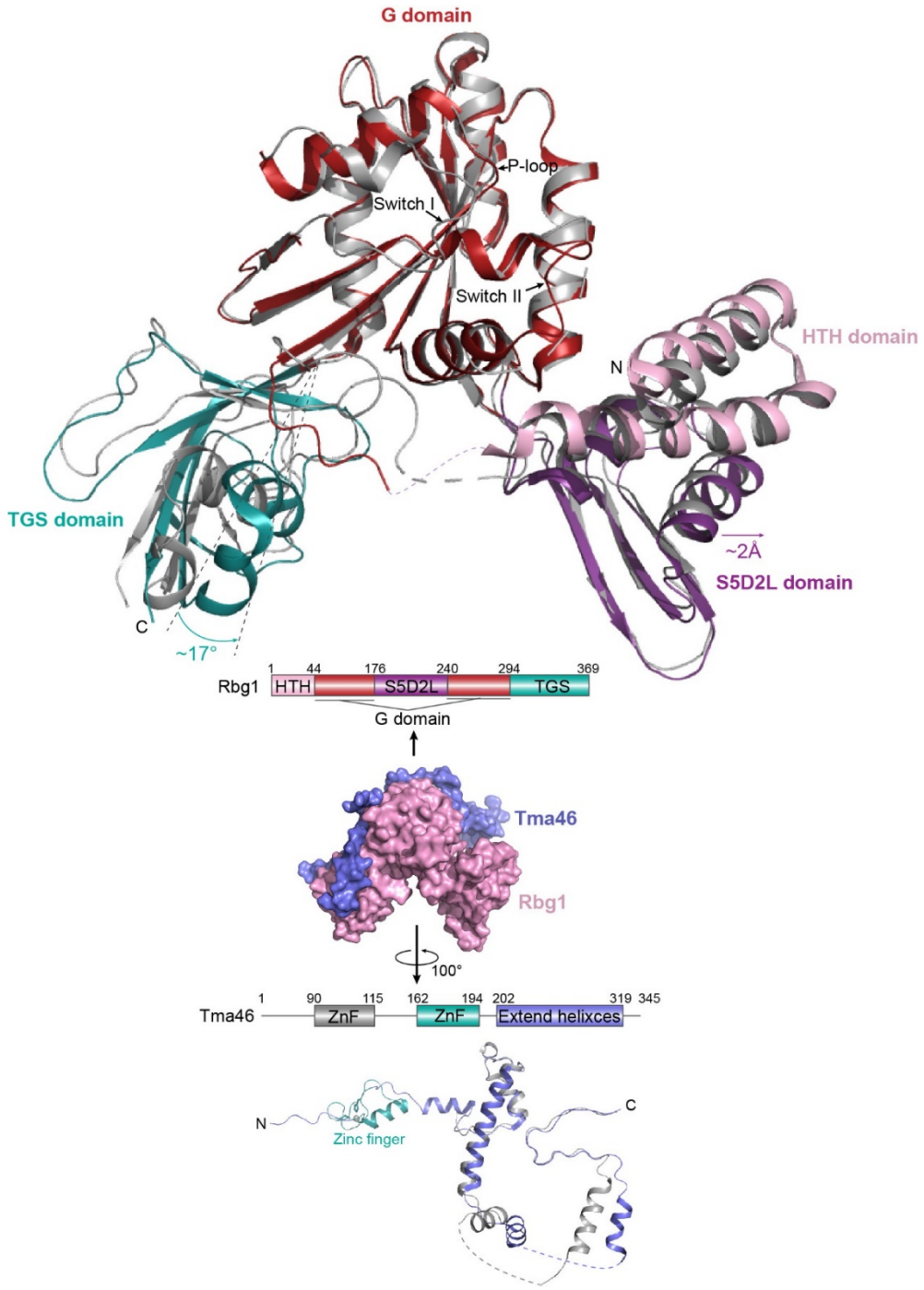

99

100 **Supplemental Figure 7. Conformation of Rbg1/Tma46 in the free form and ribosomal**

101 **complex.** Superposition of structures of Rbg1/Tma46 in the free form (PDB code: 4a9a, colored

102 in grey) and bound to the ribosome (this study, multicolored) based on the alignment of the Rbg1

G-domain. When Rbg1/Tma46 binds to ribosome, the S5D2L domain extend out about 2Å and interacts with A-tRNA, the TGS domain rotate about 17° and interacts with h16 of 18S rRNA. The conformation of Tma46 changed due to the rotation of TGS domain in Rbg1.

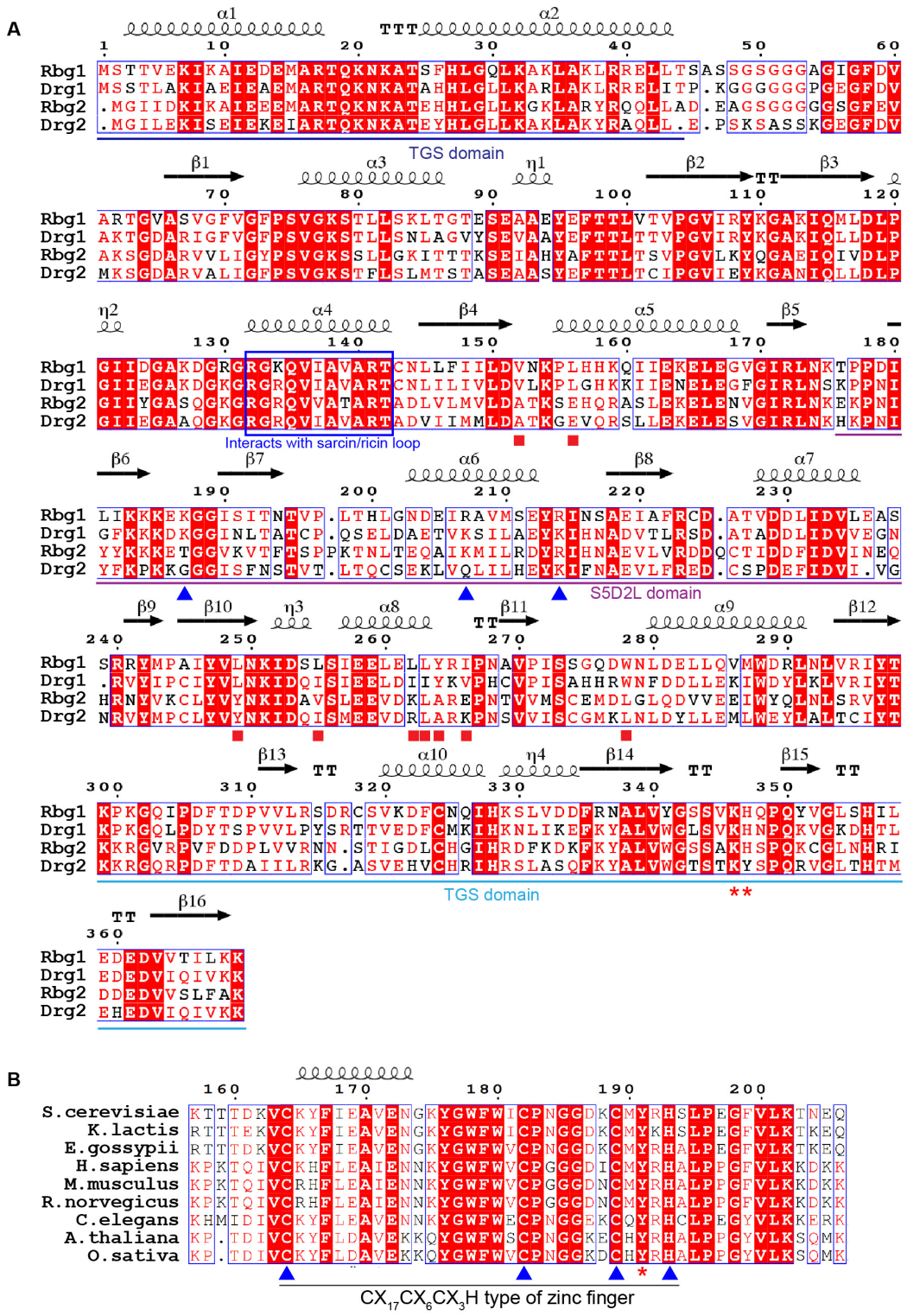

Supplemental Figure 8. Sequence alignment of Rbg1 with Rbg2 and the zinc finger region of Tma46.

110 **A.** Sequences of Rbg1 and Rbg2 in S. Cerevisiae, as well as Drg1 and Drg2 in Homo Sapiens
111 Drg1, Drg2 were aligned. Secondary structures were shown base on the structure of Rbg1
112 obtained in this study. Rbg1 residues that interact with 18S rRNA and A-tRNA were indicated
113 with the red star (*) and blue triangle (▲), respectively. The region in Rbg1 helix α4 that
114 interacts with the sarcin-ricin loop is highlighted with a blue box. Red squares (■) indicate
115 residues in Rbg1 that interact with Tma46.

116 **B.** Sequences of the second zinc finger of Tma46 in S. cerevisiae and homologues from other
117 species were aligned. The CCCH motif was labeled in blue triangle (▲) and the conserved
118 tyrosine that stacks with A506 of 16S was labeled in red star (*).

119

120 **REFERENCES**

121

122 1. Bailey, T.L. et al. MEME SUITE: tools for motif discovery and searching. Nucleic Acids
123 Res 37, W202-8 (2009).
124 2. Huang da, W., Sherman, B.T. & Lempicki, R.A. Bioinformatics enrichment tools: paths
125 toward the comprehensive functional analysis of large gene lists. Nucleic Acids Res 37,
126 1-13 (2009).

127

Supplementary Tables

Supplementary Table 1: List of yeast strains used in the study

Name	Genotype
BY4742 (WT)	*MATα his3Δ1 leu2Δ0 lys2Δ0 ura3Δ0*
Δrbg1	*MATα his3Δ1 leu2Δ0 lys2Δ0 ura3Δ0 rbg1Δ::Kana*
Δrbg2	*MATα his3Δ1 leu2Δ0 lys2Δ0 ura3Δ0 rbg2Δ::Kana*
Δrbg2Δslh1	*MATα his3Δ1 leu2Δ0 lys2Δ0 ura3Δ0 rbg2Δ::LEU2 slh1Δ::HIS3*
Δrbg2Δslh1-Rbg1d	*MATα his3Δ1 leu2Δ0 lys2Δ0 ura3Δ0 rbg2Δ::LEU2 slh1Δ::HIS3 rbg1::Kana-GAL10p-mAID-Flag*
Rbg1-TAP	*MATα his3Δ1 leu2Δ0 lys2Δ0 ura3Δ0 rbg1::rbg1-TAP-URA3*

8
9 **Supplementary Table 2**. List of Plasmids used in the study
10

Name	Details
pGAL10-mAID	Sequences including a KanMX selection marker, GAL10p, and mAID-3xFlag were inserted into the pET22b vector sequentially. Used to insert the mAID-3xFlag into the N-terminal of Rbg1 chromosomally.
p415G-TAP-URA3	TAP tag, followed by a URA3 selection marker were inserted into the multiple cloning site of the p415 vector. Used to insert the TAP tag into the C-terminal of Rbg1 chromosomally.
pPGK1	Empty vector modified from p415G, in which the GAL10 promoter was replaced by PGK1 promoter.
pPGK1-Rbg1	Overexpress the wildtype Rbg1 using a PGK1 promoter in the Δrbg1 strain to restore the Rbg1 protein level.
pET28a-Rbg1	Co-overexpress Rbg1/Tma46 in *E.coli* BL21(DE3) cells.
pET22b-Tma46	
pET22b-Tma46ΔZnF	Co-overexpress with pET28a-Rbg1 in *E.coli* BL21(DE3) cells to obtain the Rbg1/Tma46ΔZnF complex.

11
12

13
14 **Supplementary Table 3**: List of oligonucleotides used in the study
15

Name	Sequence
rP5_RND	CTTTCCCTACACGACGCTCTTCCGATrCrU**rNrNrNrNrNrNrNrN**
BioNotI-P5-PET	/5Biosg/TATAGCGGCCGCAATGATACGGCGACCACCGAGATCTACACTCTTTCCCTACACGACGCTCTTCCGATCT
P7MPX_linker_for	GTGACTGGAGTTCAGACGTGTGCTCTTCCGATCT
P7MPX_linker_rev	/5Phos/GATCGGAAGAGCACACGTCTGAACTCCAGTCAC/AmC7/
PE1.0	ATGATACGGCGACCACCGAGATCTACACTCTTTCCCTACACGACGCTCTTCCGATCT
PE2_MPX_01	CAAGCAGAAGACGGCATACGAGATCGTGATGTGACTGGAGTTCAGACGTGTGCTCTTCCGATCT
PE2_MPX_02	CAAGCAGAAGACGGCATACGAGATACATCGGTGACTGGAGTTCAGACGTGTGCTCTTCCGATCT
PE2_MPX_03	CAAGCAGAAGACGGCATACGAGATGCCTAAGTGACTGGAGTTCAGACGTGTGCTCTTCCGATCT
PE2_MPX_04	CAAGCAGAAGACGGCATACGAGATTGGTCAGTGACTGGAGTTCAGACGTGTGCTCTTCCGATCT
PE2_MPX_05	CAAGCAGAAGACGGCATACGAGATCACTGTGTGACTGGAGTTCAGACGTGTGCTCTTCCGATCT
PE2_MPX_06	CAAGCAGAAGACGGCATACGAGATATTGGCGTGACTGGAGTTCAGACGTGTGCTCTTCCGATCT
PE2_MPX_07	CAAGCAGAAGACGGCATACGAGATGATCTGGTGACTGGAGTTCAGACGTGTGCTCTTCCGATCT
PE2_MPX_08	CAAGCAGAAGACGGCATACGAGATTCAAGTGTGACTGGAGTTCAGACGTGTGCTCTTCCGATCT

16
17 /5Phos/ refers to 5’ Phosphorylation; /5Biosg/ refers to 5’ Biotine; /AmC7/ refers to 3’ Amine C7;
18 /5rApp/ refers to 5’ Adenylation; /3ddC/ refers 3’ Dideoxycytidine; bases precede by “r” refer to
19 ribonucleotides; Sequences are represented in 5’ to 3’ direction.
20
21
22

23 **Supplementary Table 4**: Data collection and model statistics
24

Data Collection	
Particles	1,222,865
Pixel size (Å)	1.08
Defocus range (μm)	-0.7 to -3.0
Voltage (kV)	300
Electron dose ($e^{-}Å^{-2}$)	30
Model composition	
Non-hydrogen atoms	212,595
Protein residues	12,322
RNA bases	5,441
Ligands (Zn^{2+}/Mg^{2+})	8/290
Refinement	
Resolution (Å)	3.23
Map sharpening B-factor ($Å^2$)	-11
FSC	0.88
Rms deviations	
Bond lengths (Å)	0.008
Bond angles (°)	0.807
Validation (proteins)	
Molprobity score	2.12
Clashscore, all atoms	12.07
Rotamer outliers (%)	0.03
Ramachandran plot	
Favored (%)	90.67
Outlier (%)	0.38
Validation (RNA)	
Correct sugar puckers (%)	98.42%
Good backbone conformations (%)	79.53%

25
26